Norwegian University of Life Sciences

Master's Thesis 2023 30 ECTS
Faculty of Science and Technology (REALTEK)

Experimental Investigations of Pure Wood Connections

Marius Backe
Structural Engineering and Architecture

Abstract

A well adopted timber-to-timber connection type in Scandinavia is the one with slotted-in steel plates and steel fasteners. The following study investigated the possibility of adopting this type of connection, substituting steel components with wood. The fact that pure wood connections have a lower environmental impact contrary to one that utilizes steel for the plates and fasteners, presents no novelty. Not only could it lower the submission of greenhouse gases as it could lower the production of steel, but it could also positively affect the cost, weight, and esthetics of a structure. An additional advantage linked to wood is better fire resistance abilities compared to steel.

In this study experimental investigations of pure wood connections were conducted by substituting the steel plates and fasteners with gusset plates of birch plywood and laminated densified wood dowels. Previous studies have investigated laminated densified wood, which proved that the material possesses impressive capacities. This study aimed to evaluate whether laminated densified wood had potential as a fastener in a timber-to-timber multiple shear connection. For the sake of comparison, two additional test groups were made, one with steel screws, and one with birch dowels. A tensile load was applied to the connections, and the load-deformation behavior was recorded. Additionally, analytical models for calculating the total capacity of multiple shear connections were presented. The calculated results according to these models were compared to the experimental results.

The research found that laminated densified wood posed as a promising material for wood dowels in terms of its impressive strength. Laminated densified wood dowels showed comparable strengths to steel screws, and higher strengths than birch dowels. Comparison between the results from the analytical calculations and the experiments showed reasonable utilization ratios, but also room for further optimizations of the models.

Keywords: laminated densified wood, birch, dowels, plywood, Glulam, multiple shear connection, timber-to-timber connection.

Preface

This master's thesis represents my final assignment as a Structural Engineering and Architecture graduate student at The Norwegian University of Life Sciences. I am thankful for the opportunity to delve into the experimental investigations and research of a pure wood connection.

I would like to extend my gratitude to my supervisors Prof. Roberto Tomasi (NMBU) and Prof. Roberto Crocetti (KTH). I am thankful for all the time and dedication, critical insight, and great feedback throughout this process. I am humbled by the extent of assistance provided. Thank you Roar Økseter, Xiaojun Gu, Anders Q. Nyrud, for the time, assistance, and expertise in the laboratory. An additional thanks to Øyvind Hansen, with co-workers, at the mechanical workshop for the assembling of pieces for the test setup.

Moreover, I would like to thank Morten Tobiassen, along with the workers at Aanesland Treindustri that helped with the construction of the specimens and Ona Flindall, Jørgen Tycho and Katrin Wilde-Sampaio, at Oslotre for their collaboration, genuine interest and time invested in the project.

Last but not least, I would like to thank my dear friends and family who have supported and encouraged me throughout my time as a student.

Oslo, July 2023

Marius Backe

Table of Contents

Abstract II
Preface IV
Table of Contents V
List of Tables VII
List of Figures VIII
Abbreviations and Acronyms XI
1 Introduction 1
1.1 Background 1
1.2 Aims and Objectives 2
1.3 Earlier Work 3
2 Theoretical Framework 6
2.1 Wood as a Construction Material 6
2.2 Glue Laminated Timber 7
2.3 Plywood 8
2.4 Birch 8
2.5 Lignostone® Transformerwood® Laminated Densified Wood 9
2.6 Strength of Multiple Shear Connections According to Eurocode 5 10
2.7 Timber Joint Design with Wood Dowels 13
2.7.1 Influence of Density- and Slenderness Ratios on Timber Pegged Joint Behavior 14
2.7.2 Ductility 15
2.7.3 Theoretical Strength of Connections with Wood Dowels 16
3 Materials and Methods 19
3.1 Materials and Dimensions 19
3.2 Testing Procedure According to NS-ISO 6891:1991 22
3.3 Data Processing in Python and Excel 24
3.4 Test Machine and Test Setup 25
3.5 Test Groups 30
3.6 Density and Moisture Content of the BD- and LDW-Dowels 31
4 Results 33

4.1 Results from the Experimental Investigations of the BD-tests 33
4.2 Results from the Experimental Investigations of the LDW-tests 37
4.3 Results from the Experimental Investigations of the S-tests 40
4.4 Density and Moisture Content Results 43
4.5 Summary Results According to NS-ISO 6891:1991 44
5 Discussion 45
5.1 Evaluation of the Overall Force-Deformation Behavior of the Tension Tests 45
5.2 Discussion of the Ductility Ratio 47
5.3 Failure modes 47
5.4 Experimental Results Compared to Analytical Models 51
5.5 Implications and Limitations in the Experiment 52
5.6 Further work 54
6 Conclusion 55
References 56
Appendix A – Analytical Calculations 60
Appendix B – Excel Spreadsheets – Moisture Content and Density 76
Appendix C – Python Scripts 79

List of Tables

Table 2- 1 - Mechanical properties of the specific Lignostone® Transformerwood® employed in this study. (Röchling, 2015)..... 10

Table 3- 1 – Overview of the test groups, with ID and description. 30

Table 4- 1 – Overview of specific numbers and info linked to the tests done with birch dowels. 36
Table 4- 2 – Overview of specific numbers and info linked to the tests done with LDW dowels. 39
Table 4- 3 – Overview of specific numbers and info linked to the tests done with steel screws. 42
Table 4- 4 – Overview of the measured mean, maximal and minimum densities, and moisture contents for the wood dowels from each test. 43
Table 4- 5 – Summary of the main results of interest. It follows the rules provided in NS-ISO 6891:1991. 44

Table 5- 1 – Overview of a trending increasement in strength with the increasement of density and decreasing in moisture content for the LDW-dowels. 46
Table 5- 2 – Overview of utilization rates between the estimated force from analytical calculations and measured forces from the experiments. 51

List of Figures

Figure 2- 1 – "Three principal axes of wood with respect to grain direction and growth rings." Figure and caption obtained from: (Forest Product Laboratory, 2010) 7
Figure 2- 2 – Cross-sectional illustration of GL30c component T22 and T15 represents the characteristic tensile strength grade, B is the height. (Swedish Wood, n.d.) 8
Figure 2- 3 – Key for identification of the different configurations and qualities. (Röchling Industrial , 2023) 9
Figure 2- 4 – Illustration of the different failure modes in a multiple shear timer-to-timber connection (Blaß & Sandhaas, 2017) 12
Figure 2- 5 – A step by step illustration for calculating the total load-bearing capacity of a symmetrical timber-to-timber connection with four shear planes (Blaß & Sandhaas, 2017). 13
Figure 2- 6 – Limit behavior of wood dowels; (a) strong peg, weak base material, less confinement of the peg and flexural dominated behavior; (b) weak peg, strong base material, more confinement of the peg and shear dominated (Sandoli, et al., 2023) 14
Figure 2- 7 – Illustration of the determination of the yielding- and ultimate point according to the standard ASTM D5764-97a (Sandoli, et al., 2023). 15
Figure 2- 8 – Classifications for ductility for connections (Sandoli et al., 2023; Smith, et al., 2006). 15
Figure 2- 9 – Overview of The European Yield Model inspired by Eurocode 5 (Sandoli, et al., 2023). 16

Figure 3- 1 – Sketch of full test setup for the tension test. 19
Figure 3- 2 – Sketch of the tension test specimen with lengths. Light grey and brown plates; Birch plywood, yellow pieces; Glulam, dark grey pieces; steel attachment pieces, brown rods; wood dowels. 20
Figure 3- 3 – Total thickness of the specimen, t=264mm, t1 = 21mm and t2=90mm. 20
Figure 3- 4 – Detailed drawings of the middle plywood plates, Glulam pieces and end plywood plates. 21
Figure 3- 5 – Detailed drawing of the wood dowels. 22
Figure 3- 6 - Detailed drawing of the VGZ screw from Rothoblaas (Rothoblaas, 2020). 22
Figure 3- 7 – "Loading procedure." (NS-ISO 6891:1991, 1991) 24
Figure 3-8 – The Zwick ZR1200 test machine with the prototype attached in it. 26
Figure 3-9 – Visual representation of how the specimens is restrained with a fully threaded steel dowel with a diameter of 50mm. 27
Figure 3- 10 – Illustration of the AEP LDT transducer accompanied by a table showcasing the types that was utilized for this experiment, marked with red (AEP transducers, 2020). 28
Figure 3-11 – a) and b) visual representation of the placement of the displacement gauges. They are mirrored to ensure that deformations are detected in as many parts of the specimen as possible. They are given a number, #1-4, as you can see in the pictures. 29
Figure 3-12 – Visual representation of how the clamps is attached to hold the plywood plates adjacent to the Glulam pieces. 30

Figure 4- 1 – Visual representation of the force applied, in kN, vs. the displacement, in mm, measured from sensor #1 from the test with birch dowels. Red dotted line marks 15mm. Red dots mark the maximal force. 33
Figure 4- 2 – Visual representation of the force applied, in kN, vs. the displacement, in mm, measured from sensor #2 from the tests with birch dowels. Red dotted line marks 15mm. Red dots mark the maximal force..... 34
Figure 4- 3 – Visual representation of the force, in kN, applied vs. the displacement, in mm, measured from sensor #3 from the test with birch dowels. Red dotted line marks 15mm. Red dots mark the maximal force. 34
Figure 4- 4 – Visual representation of the force, in kN, applied vs. the displacement, in mm, measured from sensor #4 from the test with birch dowels. Red dotted line marks 15mm. Red dots mark the maximal force. 35
Figure 4- 5 – Visual representation of the force applied, in kN, vs. the displacement, in mm, measured from sensor #1 from the tests with laminated densified wood dowels. Red dotted line marks 15mm. Red dots mark the maximal force. 37
Figure 4- 6 – Visual representation of the force applied, in kN, vs. the displacement, in mm, measured from sensor #2 from the tests with laminated densified wood dowels. Red dotted line marks 15mm. Red dots mark the maximal force. 37
Figure 4- 7 – Visual representation of the force applied, in kN, vs. the displacement, in mm, measured from sensor #3 from the tests with laminated densified wood dowels. Red dotted line marks 15mm. Red dots mark the maximal force. 38
Figure 4- 8 – Visual representation of the force applied, in kN, vs. the displacement, in mm, measured from sensor #4 from the tests with laminated densified wood dowels. Red dotted line marks 15mm. Red dots mark the maximal force. 38
Figure 4- 9 - Visual representation of the force applied, in kN, vs. the displacement, in mm, measured from sensor #1 from the tests with steel screws. Red dotted line marks 15mm. Red dots mark the maximal force. 40
Figure 4- 10 – Visual representation of the force applied, in kN, vs. the displacement, in mm, measured from sensor #2 from the tests with steel screws. Red dotted line marks 15mm. Red dots mark the maximal force. 40
Figure 4- 11 – Visual representation of the force applied, in kN, vs. the displacement, in mm, measured from sensor #3 from the tests with steel screws. Red dotted line marks 15mm. Red dots mark the maximal force. 41
Figure 4- 12 – Visual representation of the force applied, in kN, vs. the displacement, in mm, measured from sensor #1 from the tests with steel screws. Red dotted line marks 15mm. Red dots mark the maximal force. 41

Figure 5- 1 – Illustration of lines drawn on S-(1); (a) prior to testing; (b) after testing. 48
Figure 5- 2 – Illustrations of the extracted dowels from the BD-tests. 49
Figure 5- 3 – Illustrations of the dowels extracted from the LDW-tests. 50

Abbreviations and Acronyms

BD – Birch dowel

d – Diameter

EYM – European Yield Model

$\mathbf{F_{ax,k}}$ – Characteristic withdrawal resistance

$\mathbf{f_{c,0,m}}$ – Characteristic compressive strength parallel to grain

$\mathbf{F_{est}}$ – Estimated force

$\mathbf{F_{h,k}}$ – Embedment strength

$\mathbf{f_{m,k}}$ – Characteristic bending strength

$\mathbf{f_{u,k}}$ – Characteristic tensile strength

$\mathbf{F_{v}}$ – Shear capacity of fastener per shear plane

$\mathbf{F_{v,Rk}}$ – Characteristic capacity of the fastener per shear plane

I_s, I_m, III_s and IV – Failure modes in a multiple shear connection

L or l – Length

LDW – Laminated Densified Wood

$\mathbf{l_{ef}}$ – Threaded depth of the threaded part of the screw

m – mass

$\mathbf{m_{dry}}$ – Mass after drying

$\mathbf{m_i}$ – Initial mass

$\mathbf{m_w}$ – mass of water

$\mathbf{M_{y,k}}$ – Characteristic yielding moment of the fastener

$\mathbf{n_{ef}}$ – Number of fasteners

S – Steel screw

SP- I, II, III and IV – Shear planes; 1, 2, 3 and 4 in a multiple shear plane connection

t – Thickness

u or δ – Deformation/slip

V – Volume

$\mathbf{V_0}$ – Volume of submerged object

VGZ – Full threaded screw from Rothoblaas

$\mathbf{w_{\%}}$ **-** Moisture content in percent

α – Angle between force- and grain-direction

β – Relationship between embedment strengths

μ – Ductility

ρ – Density

$\mathbf{\rho_w}$ – Density of water

1 Introduction

The construction industry represents a substantial sector contributing to emission of GHGs (i.e, greenhouse gases), which in turn impact the climate (Labaran, et al., 2021). There is a growing need to adopt materials and methods that are environmentally friendly. The use of wood elements and structures is such an approach. Wood possesses exceptional properties that make the material highly advantageous, for instance psychical, technological, aesthetic and utility properties (Švajlenka & Kozlovská, 2021). Himes and Busby, (2020) propose wood building as a climate solution (Himes & Busby, 2020). The following study wishes to investigate a potential pure wood connection, which if successful, could increase the utilization of wood for structural purposes. The research is also in line with the expansional need to gain more knowledge concerning the employment of wood as a construction material.

1.1 Background

In Scandinavia, a well adopted connection type for heavy timber structures is the one with slotted in steel-plates and steel dowels. This type of connections/joints is frequently found in industrial buildings, sports arenas, and residential buildings. What characterizes such a connection is one or several steel plates allocated in slots made in timber members. The transmission of shear between steel and timber occurs by the means of steel dowels. One disadvantage with this method is that both the steel plates and timber members must be predrilled with holes for the dowels with a high degree of accuracy. This makes such a connection highly sensitive to misalignments as such errors often must be mended at the building site and could possibly challenge the time and economy in a building process. If such problems are handled by enlarging the predrilled holes, and thus reducing the strength and stiffness of the connection. Moreover, the slotted in steel-plate connections with steel dowels requires a large amount of steel, which again negatively affects the environment. It is therefore interesting to investigate how to “modernize” the traditional multiple shear plane steel-timber joints by replacing the steel components with wood products, and at the same time optimizing a “full-wood” connection’s strength and stiffness.

Scandinavia is home to large areas of birch forests. It is not a wood species known for a structural material but obtains characteristics that are comparable to other hardwood species which are already established as applicable materials for this purpose. Hence, it is of great interest that birch is employed in the tests conducted in this study. If the results show that birch could have a good potential as a plate and/or dowel material, this could mean a great deal in terms of a broader utilization of Scandinavian birch. Additionally, it would have a positive effect on the environment as other less accessible wood species could be replaced by a species with a shorter journey from raw material to a building component. Quite possibly, this could also affect the building cost in a positive way.

1.2 Aims and Objectives

It is evident that there is a need to develop timber to timber connections. That is, to substitute steel components with wood. As research and earlier work show, more knowledge on this field is necessary in the pursuit of building larger and more complex timber structures. Accordingly, the current thesis sought to investigate in what way, and to what extent specific wood products pose as a substitute for steel components in a multiple shear connection. More specifically, steel plates and dowels will be replaced by birch plywood and laminated densified wood. For the sake of comparison, the structural behavior of one connection with birch plywood gusset plates and steel screws, and one connection with birch plywood gusset plates and birch dowels, will also be studied. The main evaluation will be of the load-slip behavior of the tests.

As the development of massive structures free of steel moves forward, the need for new analytical models for predicting the strength and stiffness arises. Therefore, a review of suggested analytical models will be presented. Calculations according to these proposals were done to get a prediction of the results, and then compared with the results from the experimental testing.

The specific aims were to investigate the following research questions:

RQ1: How does laminated densified wood perform in comparison to steel screws and birch dowels?

RQ2: How do the proposed analytical models work in terms of estimating the capacity of a wood doweled shear plate connection?

1.3 Earlier Work

There are several investigations conducted on the use of wood dowels in timber connections, concerning the potential of different wood- and wood-based products (e.g., Larson, 2020; Furuheim & Nesse, 2020; Sandoli, 2023). Some studies even propose new design methods for projecting the strength, stiffness and other capacities of a connection consisting of wood as the only material.

A research article by Larsson (2020), explored dowel design of the shear plate dowel joints, in which laminated densified wood was tested as material for dowels. The laminated densified wood dowels were compared to other types of dowels, including metal dowels. According to the study laminated densified wood performed similar to metal dowels in terms of strength, stiffness, and hardness, making it a highly capable product for large load transfers. For this reason, it was of high interest to use this material for the experiments conducted in this thesis. Since the contact information of the manufacturer of this product was provided by Larsson in the paper, laminated densified wood from Röchling was used (Larsson, 2020).

A study by Sandoli and colleges (2023) investigated the feasibility of using timber pegged joints in modern seismic-resistant structures or for upgrading existing structures. Doweled connections and their behavior have been examined for many years, but evaluation of the seismic design aspects deficient. Sandoli et al. (2023) gathered data for a database with over 350 test results from previous studies. The purpose of the study was to analyze the data, define seismic design aspects and design a model more suitable for wood doweled connections that are easily employed in an engineering practice. This included an analysis of the effectiveness of the European Yield Model (EYM) for calculating the maximal strength of connections with wood dowels, especially regarding the embedment strength. Results proved that wood dowels perform as a good substitute for steel-doweled connections, and thus have a great potential in a seismic-resistant structure. Data processing also resulted in the discovery of a suitable value for the overstrength factor, which can help project the joint capacity, and establishes reasonable range of

ductility classes. In the end, the study emphasized that the European Yield Model proved to be a practical way to calculate connection strength. However, given that it employes wood dowels as fasteners, Sandoli et al. propose that the model needs to be slightly modified. Further, the research suggests a new equation to calculate the embedment strength, and to use other material characteristic values to calculate the yielding moment of wood fasteners (Sandoli, et al., 2023).

Miller and Schmidt (2004) conducted a study concerning connections of pegged mortise and tenon joints. Several tests were performed, and Finite Element Modeling (FYM) was conducted to develop a design method for the shear strength of wood dowels. Correlation between the shear strength and the specific gravity of the materials led to an equation for calculating the shear yield stress per shear plane in the joint (Miller & Schmidt, 2004).

A previous study investigated beam-column connections in glulam structures, with gusset Plates of birch plywood and self-tapping screws (Furuheim & Nesse, 2020). Different configurations of the employed materials were tested. Additionally, the results from the experimental investigations were evaluated for its use in real design. The thesis contains methods and material characteristics which are useful in the assessment of pure wood connections.

A paper by Crocetti et al. (2020), presents results from an experimental study on multiple shear joints consisting of gusset plates, either made from LVL or plywood connected to timber members with full threaded self-tapping screws. Investigations of different types of wood for the gusset plates, their face grain orientation, and their thickness, showed promising values for structural performance. The authors emphasize that the mentioned materials pose as a good replacement for the traditional connections made with slotted-in steel plates and steel dowels (Crocetti, et al., 2020). Moreover, the paper includes relevant materials and methods for this thesis. Firstly, it employes birch plywood as one of the materials used as gusset plates. Secondly, the test setup for this thesis is somewhat adopted from the experiments conducted by Crocetti et al. (2020).

Kromoser et al. (2021), discussed the importance of structural optimization in wood construction to efficiently utilize wood and wood-based materials. Minimizing material quantity and a focus on resource-saving strategies are highlighted. The paper accentuates the potential benefits of using wood for all construction components, including connections such as cost reduction, improved ecological impact, and enhanced fire resistance. The specific focus of the paper is on

the optimization of truss geometry and connections using wood as the sole construction material. A parametric model and a genetic solving algorithm are employed to reduce the required construction material. The wood-wood connection is established using birch- and beech plywood and wooden pegs from different species, in the nodes of the truss. Tensile investigations reveal that beech pegs provide the stiffest and highest load-bearing capacity connection. Compression tests were conducted to assess local buckling failure in the plywood panel, considering the influence of free length. In accordance with the authors, it is noteworthy to mention that the relationship between the peg/dowel diameter and thickness of the plywood needs to be carefully evaluated to ensure ductile failure of the connection (Kromoser, et al., 2021).

2 Theoretical Framework

This chapter will delve into the associated materials and timber mechanics, to form a framework for the study's aim of investigation. Following, this will include basic aspects of wood, glulam, plywood, birch, laminated densified wood, and their characteristics. Lastly, the theory concerning the analytical models meant for determining the capacity of multiple shear connections, for the respective fasteners, is elaborated.

2.1 Wood as a Construction Material

As a building material wood possesses excellent properties. Simple production and local access to raw materials is historically what makes timber our most valuable resource for construction materials (Edvardsen & Ramstad, 2014). Timber is associated with a high strength to weight ratio, making it a good material for long spans. On the other hand, timber differs from homogenous materials like concrete and steel, making it a complex material to work with.

In contrast to steel and concrete, wood is described as an orthotropic material. What this implies is that it has different capacities in different directions, which need to be accounted for. Wood can be divided into three axes, namely the longitudinal axis, the radial axis, and the tangential axis. The axes are shown in Figure 2-1. The longitudinal direction of timber is often referred to as the fiber or grain direction, while the radial and tangential direction is referred to as the direction perpendicular to the fiber or grain (Forest Product Laboratory, 2010).

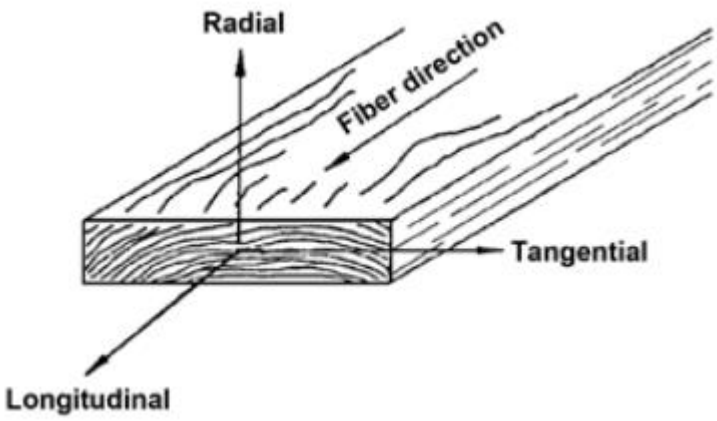

Figure 2- 1 *– "Three principal axes of wood with respect to grain direction and growth rings." Figure and caption obtained from: (Forest Product Laboratory, 2010)*

Moisture content in timber affects its capacities. When the moisture content gets closer to the fiber saturation point, which is approximately at 30%, the strength will decrease. As the timber dries, the strength increases. Naturally dried wood will normally maintain a moisture content of approximately 12%, which also reflects what the desired value should be in timber construction members. Other factors affecting the strength negatively are load duration, twigs interfering with the grain direction, and increasing temperatures (Edvardsen & Ramstad, 2014).

2.2 Glue Laminated Timber

Glue Laminated Timber, GLT, or Glulam consists of layered lamellas of assorted strength classes glued upon each other. In Norway, mainly spruce is utilized for Glulam, as well as pine. The lamellas are often finger jointed together. They usually consist of 4 lamellas or more, with an approximate thickness of 45mm or less (Edvardsen & Ramstad, 2014). One of the most common strength classes for structural components is GL30c. The value 30 in GL30c is the characteristic bending strength of the Glulam. The "c" indicates that the lamellas consist of combined strength classes. Maximal tensile and compressive stresses occur in the upper and lower part and is the reason for why Glulam often consists of lamellas of different strength classes in the middle and outer parts. However, Glulam is also available with a homogeneous cross-section, represented with an "h" (Swedish Wood, n.d.).

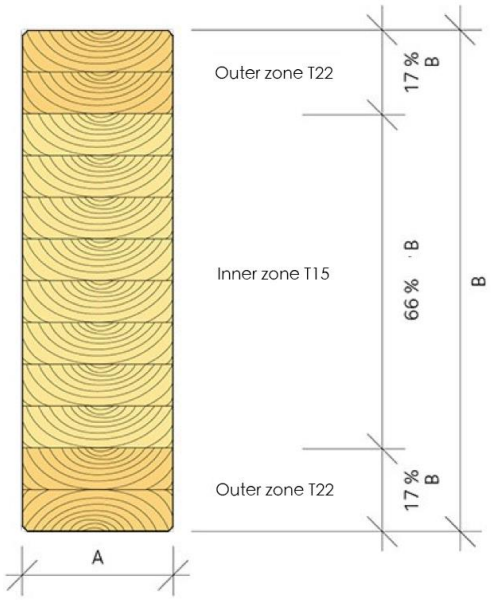

Figure 2- 2 *– Cross-sectional illustration of GL30c component T22 and T15 represents the characteristic tensile strength grade, B is the height. (Swedish Wood, n.d.)*

2.3 Plywood

Plywood is a wood product made from thinly layered veneers glued together. Birch plywood normally consists of layers of 1,4 millimeters. Whereas for softwoods, like spruce, the thickness of the layers varies from l,4-3,2 millimeters. Birch plywood usually has a characteristic value of approximately 680 kg/m^3. It is typical for hardwoods, like birch, to have a higher density than softwoods. and. Plywood made with spruce has a density of 450-500 kg/m^3 (Furuheim & Nesse, 2020), while beech plywood have a density of approximately 800 kg/m^3 (Crocetti, et al., 2020).

2.4 Birch

According to a paper written by Boruvka et al. (2018) birch as an unprocessed material has a minimum density of 510 kg/m^3, a mean density of 650 kg/m^3 and a maximum density of 830 kg/m^3. The same paper states that birch has a mean bending strength of 147 MPa. Birch has a compressive strength parallel to the grain of 39,2-58,9 MPa (The Engineering ToolBox, 2011). However, the compressive strength applies to paper-, sweet- and yellow birch, so one must account for slightly different values for birch-species found in Scandinavia.

2.5 Lignostone® Transformerwood® Laminated Densified Wood

Röchling Industrial claims to be the inventor and world market leader in producing laminated densified wood, having produced Lignostone® for over a century. Primarily, Lignostone® Transformerwood® serves a great purpose as a material used in transformers, as it meets the high electrical and thermal requirements for this application. Lignostone® Transformerwood® is a laminated densified wood according to IEC 61061. It consists of thinly layered veneers. The wood species used for the veneers are red beech. The veneer layers are glued together with a thermosetting synthetic resin before applying high pressure and heat. Red beech obtains excellent electrical and mechanical characteristics, with respect to the use as insulation material in oil-filled transformers. However, the mechanical properties can make the material suitable for structural components as well. Lignostone® Transformerwood® obtains promising characteristics with its high strength and stiffness. Some characteristics are listed below, in Table 2-1. It is worth mentioning that in pursuance of making Lignostone® Transformerwood® as environmentally friendly as possible they make sure to only purchase veneers from suppliers that are certified in accordance with the regulations of the Forest Stewardship Council (FCS®). Further on, the use for this application is to employ the material for dowels in a multiple shear connection. The company provides a selection of different configurations and classes. Round rods are listed in their industrial folders and can be delivered in a standard length of 2000mm and diameters from 6-28mm. The industrial folder also provides a key to identify the different configurations. Figure 2-3 describes the key to identification. (Röchling Industrial , 2023).

	Key	Explanation	
Degree of density	L	Low density	Specific gravity: 0.75 – 1.10 g/cm³
	M	Medium density	Specific gravity: 1.10 – 1.30 g/cm³
	H	High density	Specific gravity: 1.30 – 1.40 g/cm³
Lamination	I	Parallel	
	II	Crosswise	
	X	Tangential	
Veneer thickness	2	≥ 2 mm	
Resin	E3	Resin for electrical applications	
Veneer quality	(SQ)	Standard quality	Field strength E at onset of PD: **3.3 kV/mm**[1] **Fulfills** the requirements of IEC 61061
	(HQ)	High Quality	Field strength E at onset of PD: **4.7 kV/mm**[1] **Surpasses** the requirements of IEC 61061
	(TQ)	Top Quality	Field strength E at onset of PD: **5.1 kV/mm**[1] **Surpasses by far** the requirements of IEC 61061

Example: LII/2-E3 (SQ) means:
- Low density
- Crosswise lamination
- Veneer thickness ≥ 2 mm
- Electric type
- Standard quality

Figure 2- 3 *– Key for identification of the different configurations and qualities. (Röchling Industrial , 2023)*

***Table 2- 1** - Mechanical properties of the specific Lignostone® Transformerwood® employed in this study. (Röchling, 2015)*

ID	MI/2-E3
Density [kg/m^3]	>1350
Flexural strength [MPa]	200
Modulus of elasticity in flexure [GPa]	16
Compressive strength perpendicular to grain [MPa]	120
Compressive strength parallel to grain [MPa]	90
Tensile strength parallel to grain [MPa]	170
Moisture content [%]	5
Illustration	Parallel packed 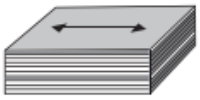

2.6 Strength of Multiple Shear Connections According to Eurocode 5

Eurocode 5 provides a well incorporated method for calculating the strength of timber-to-timber multiple shear connections using the Johansen approach. For a timber to timber double shear connection the characteristic capacity of the fastener per shear plane, $F_{v,Rk}$, should be calculated for different failure modes (NS-EN 1995-1-1:2004, 2004). This part of the thesis will enlighten how the strength of a timber-to-timber multiple shear connection with full threaded screws is calculated, accounting for the rope effect. Mainly three parameters are important to account for when calculating the strength of a connection: (1) the embedment strength of the timber, (2) the withdrawal resistance of the fastener, (3) the fasteners yielding moment (Furuheim & Nesse, 2020).

The embedment strength of the timber refers to the capacity of the wood in compression where stress from the fastener is applied. The parameters for calculating the embedment strength are density of the timber components, diameter of the fastener, the angle between the force and grain direction, the area of the wood in contact with the fastener. The embedment strength of glulam and plywood is calculated differently. Plywood only accounts for the density of the plate, as the grain direction does not make any difference (Furuheim & Nesse, 2020; NS-EN 1995-1-1:2004, 2004).

Eurocode 5 provides a method of calculating the withdrawal resistance, $F_{ax,k}$. However, for this study the withdrawal resistance of the employed screws was provided in a data sheet from the manufacturer, and it was used in the calculation for projecting the capacity of the tests with steel screws. Dowels are not known to have a withdrawal resistance, as they have a smooth surface. Briefly explained, the withdrawal capacity refers to the strength it takes to pull out the fastener from the connection. This is only accounted for with threaded screws. Furthermore, the withdrawal resistance is used to account for the Rope effect. The rope effect increases the capacity of the connection by restraining the connection laterally. A self-tapping full threaded screw can potentially add 100% rope effect to the connection, whereas a dowel is said to not contribute at all (Blaß & Sandhaas, 2017; Furuheim & Nesse, 2020; NS-EN 1995-1-1:2004, 2004).

When load is applied to a connection, a moment causing the fastener to yield may occur. This is referred to as M_{yk} and may as well be the reason for failure in the connection. When a large enough load is applied, steel will start to yield, when this happens in joints it causes what is commonly known as a plastic hinge. The fastener's yielding moment is dependent on the diameter- and the quality of the steel- in the fastener difference (Furuheim & Nesse, 2020; NS-EN 1995-1-1:2004, 2004). However, the manufacturer of the screws used for this research is provided in a data sheet, and it is this value that is accounted for in the calculations.

Additionally, minimal distances between fasteners, end grains and edges need to be accounted for. The distances are determined depending on the fastener diameter and the angle between the load- and the fiber-direction. For some fastener types it also depends on whether predrilled holes have been made or not, and the density of the timber (NS-EN 1995-1-1:2004, 2004).

The mentioned characteristic values above can be used when projecting the strength of a connection. The Johansen approach applies these values in different configurations making equations for different failure modes. The mode with the lowest capacity is used to project the strength of the connection. Blaß & Sandhaas (2017) provides a figure illustrating the different failure modes for a multiple shear connection, see Figure 2-4.

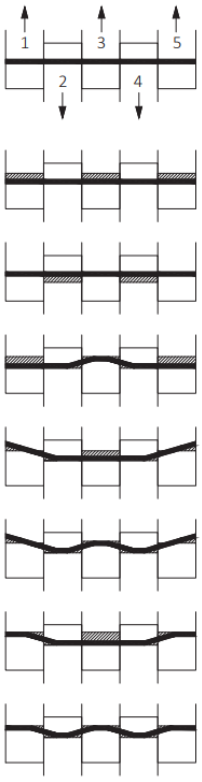

Figure 2- 4 *– Illustration of the different failure modes in a multiple shear timer-to-timber connection (Blaß & Sandhaas, 2017).*

Multiple shear connections may be looked at as a series of shear planes in a double shear connection (NS-EN 1995-1-1:2004, 2004). Blaß & Sandhaas (2017), illustrates the shear planes and how the geometry should be accounted for, see Figure 2-5.

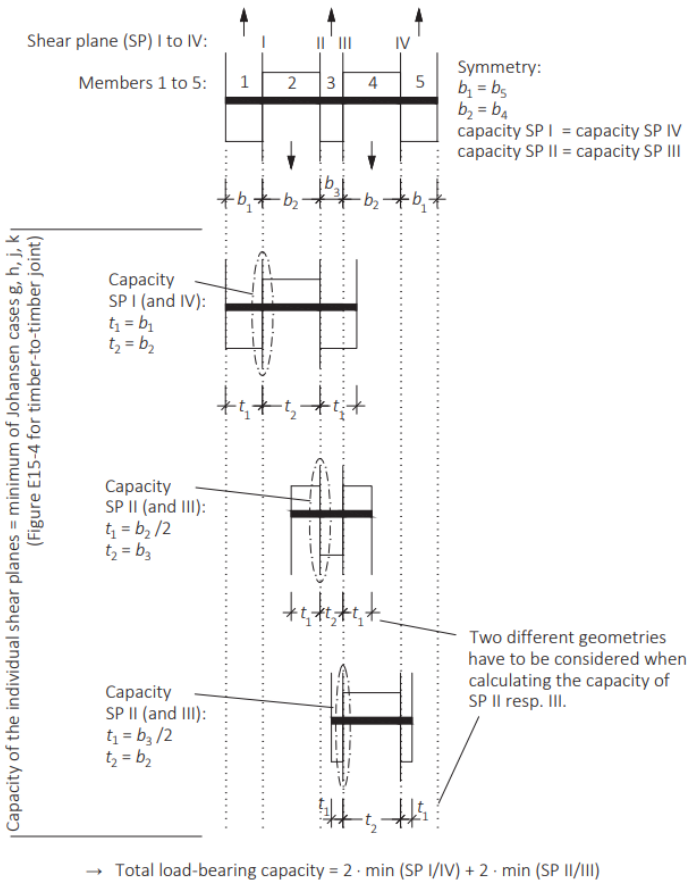

Figure 2- 5 *– A step by step illustration for calculating the total load-bearing capacity of a symmetrical timber-to-timber connection with four shear planes (Blaß & Sandhaas, 2017).*

2.7 Timber Joint Design with Wood Dowels

Designing a multiple shear connection with timber pegs can, according to Sandoli et al. (2023), be done with the same approach as the one explained in Chapter 2.6. However, Sandoli et al. (2023), emphasizes the need to make modifications to the European Yield model to make it suitable for timber pegs. These modifications will be delved into in the following sections.

2.7.1 Influence of Density- and Slenderness Ratios on Timber Pegged Joint Behavior

Overall, it can be said that the shear behavior of timber pegs is significantly influenced by either the density ratio or slenderness ratio (t_{min}/d), depending on behaviors between force and displacement, and failure mechanisms of the connections. Sandoli et al. (2023), identifies two limit behaviors; (a) strong peg in weak base material, (b) weak peg in strong base material. The authors illustrate a figure representing these limits, see Figure 2-6. Case (a) shows less confinement of the peg and can be achieved if the peg density is higher than the base material density, or when the peg diameter increases with respect to the base material thickness. Case (b) shows more confinement of the peg and can be achieved if the peg density is lower than the base material density, or when the peg diameter decreases with respect to the base material thickness. Evaluation of the free length, L, shows a longer deformation for case (a) than (b). According to Sandoli et al. (2023), this implies a more flexural-dominated behavior in case (a), and a more shear-dominated behavior in case (b). It is also states that pegs with shear dominated behavior have the higher load-bearing capacity between these two cases (Sandoli, et al., 2023).

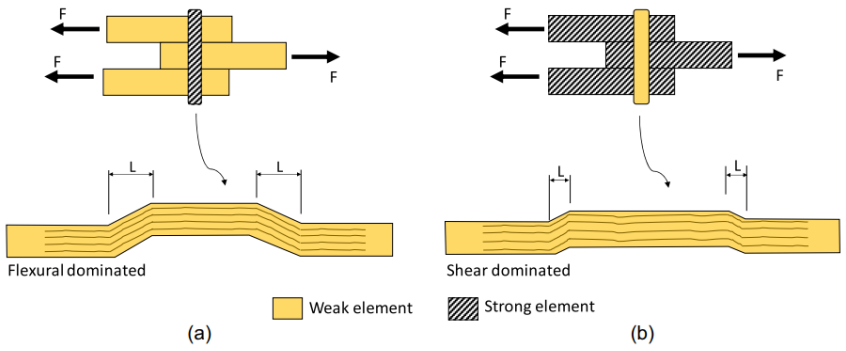

Figure 2- 6 *– Limit behavior of wood dowels; (a) strong peg, weak base material, less confinement of the peg and flexural dominated behavior; (b) weak peg, strong base material, more confinement of the peg and shear dominated (Sandoli, et al., 2023).*

2.7.2 Ductility

The ductility, μ, of a connection can be described as the ability to surveil large deformations within the plastic range without considerable reduction of strength, and it can be calculated as the ratio between the ultimate deformation, u_u, and the deformation when the connection transitions from an elastic behavior to plastic behavior, u_y. However, Sandoli et al. (2023), emphasizes that there are many methods for deciding where the yielding point is on a force-displacement graph. Having presented several methods, Sandoli et. al, calculated the yielding point according to the procedure given by the standard ASTM D5764-97a (ASTM, 2013): an offset of 5% of the fastener diameter from a line passing from the origin of the axes through the point of 40 % of F_{max}, as illustrated in Figure 2-7. The same figure shows how they found the ultimate point, u_u, as well (Sandoli, et al., 2023).

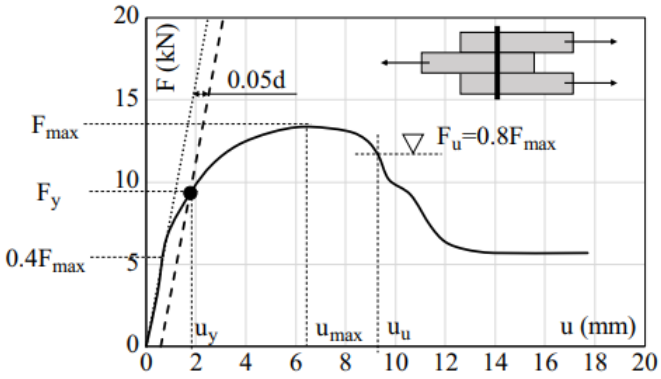

Figure 2- 7 *– Illustration of the determination of the yielding- and ultimate point according to the standard ASTM D5764-97a (Sandoli, et al., 2023).*

A classification model for ductility is presented in Figure 2-8 (Sandoli et al., 2023; Smith, et al., 2006).

Classification	Average ductility
Brittle	$\mu \leq 2$
Low ductility	$2 \leq \mu \leq 4$
Moderate ductility	$4 \leq \mu \leq 6$
High ductility	$\mu \geq 6$

Figure 2- 8 *– Classifications for ductility for connections (Sandoli et al., 2023; Smith, et al., 2006).*

2.7.3 Theoretical Strength of Connections with Wood Dowels

Mode	Strength	Failure mode
I_s	$R_{1k} = f_{h,1,k} t_1 d$	
I_m	$R_{2k} = 0.5 f_{h,2,k} t_2 d$	
III_s	$R_{3k} = 1.05 \frac{f_{h,1,k} t_2 d}{2+\beta} \left[\sqrt{2\beta(1+\beta) + \frac{4\beta(2+\beta) M_{y,k}}{f_{h,1,k} d t_1^2}} - \beta \right]$	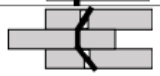
IV	$R_{4k} = 1.15 \sqrt{\frac{2\beta}{1+\beta}} \sqrt{2 M_{y,k} f_{h,1,k} d}$	

($f_{hk,1,k}$, $f_{hk,2}$ = embedding strength of timber; t_1, t_2= boards' thickness; d= fastener's diameter, $M_{y,k}$= characteristic yielding moment of the fastener, $\beta = f_{h,k1}/f_{h,k2}$)

Figure 2- 9 *– Overview of The European Yield Model inspired by Eurocode 5 (Sandoli, et al., 2023).*

The European Yield Model, EYM, also referred to as the Johansen approach, can be feasible to calculate the strength of a connection with wood dowels as long as two factors are modified and one added. It accounts for four failure modes, which is illustrated in Figure 2-9. Modes (I_s) and (I_m) represent a failure due to embedment in the base material, "s" refers to the side plates and "m" refers to the middle plates. Mode (III_s) represent failure due to embedment in all members and one plastic hinge in the fastener. Mode (IV) represents a failure due to embedment in all members and three plastic hinges in the fastener (Blaß & Sandhaas, 2017). As a part of the study conducted by Sandoli et al. (2023), it was suggested that the equations for calculating the yielding moment of wood dowels and the embedment strength should be modified when calculating the strength of a timber-to-timber connection with wood dowels. Additionally, a fifth failure mode, mode (V) which represents shear failure of the wood dowel, should be considered (Sandoli, et al., 2023).

The traditional way to calculate the yielding moment for steel dowels is according to Eurocode 5 provided with the formula given in Eq. 2-1 where $f_{u,k}$ is the characteristic tensile strength of the fastener and d is the fastener diameter (NS-EN 1995-1-1:2004, 2004).

$$M_{yk} = 0{,}3 f_{u,k} d^{2,6}$$

Eq. 2- 1 *– Yielding moment according to Eurocode 5 [Nmm] (NS-EN 1995-1-1:2004, 2004).*

Further, Sandoli et al. (2023), suggests that substituting the characteristic tensile strength, $f_{u,k,}$ with the mean compression strength parallel to the grain, $f_{c,0,m}$, will provide a suitable value for the yielding moment. The embedment strength should, according to Eurocode 5, be calculated by the equation given in Eq. 2-2 where d is the diameter of the dowel and ρ_b is the density of the base material (Sandoli, et al., 2023).

$$f_{h,k} = 0{,}082(1 - 0{,}01d)\rho_b$$

Eq. 2- 2 *– Embedment strength according to Eurocode 5 [MPa] (NS-EN 1995-1-1:2004, 2004).*

Sandoli et. al (2023) propose a more suitable equation for the embedment strength than the one provided in Eurocode 5. It accounts for both the density of the dowel, ρ_p, and the density of the base material, ρ_b, as well as the diameter of the dowel. See Eq. 2-3 (Blaß, et al., 1999; Sandoli et al., 2023).

$$f_{h,k} = \rho_b \rho_p 10^{-4} 1{,}222(1 - 0{,}011d)$$

Eq. 2- 3 *– Embedment strength suitable for timber-to-timber connections with wood dowels (Blaß, et al., 1999; Sandoli et al., 2023).*

Lastly, Sandoli et al. (2023), advocate a third factor that needs to be considered when calculating a timber-to-timber connection with wood dowels, and that is the shear strength of the dowel. This adds a fifth failure mode, Mode V, to the approach of calculating the connection strength. This failure mode could be substituted with the fourth failure mode, Mode IV, because Mode IV cannot be developed before the effective shear of the wood dowel. Plastic hinges in the wood dowel do not occur before the yielding shear (Sandoli, et al., 2023). Some equations for

calculating the shear capacity of the dowel are presented by Sandoli et al. (2023). However, another equation is employed for the purpose of projecting the shear strength in this thesis. It is provided by the paper presented in Chapter 1.3, by Miller & Schmidt (2004), see Eq. 2-4.

$$F_{vy} = 4810 G_{peg}^{0,926} G_{base}^{0,778}$$

Eq. 2- 4 *– Equation for the shear yield strength in psi, where G_{peg} refers to the specific gravity of the peg and G_{base} refer to the specific gravity of the base material. (Miller & Schmidt, 2004).*

3 Materials and Methods

The following chapter will review the test methods, materials, test groups and equipment used for this thesis. Primarily, what will be referred to as a tension test was conducted. To contribute to the depth of the experiment, measurements of moisture content and density of the wood dowels were also executed. Assembly and delivery of the specimens was conducted by collaborators for this thesis, and the construction of the test setups was conducted by the mechanical workshop at NMBU.

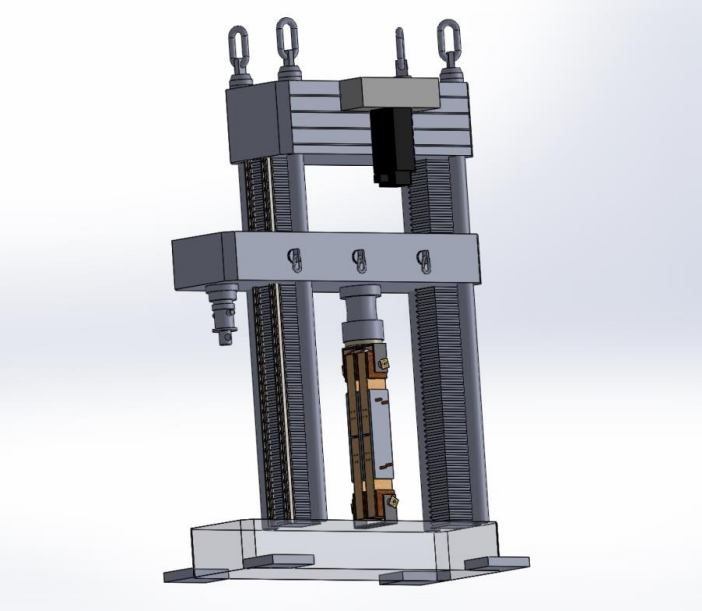

Figure 3- 1 *– Sketch of full test setup for the tension test.*

3.1 Materials and Dimensions

Materials used are the same for all specimens, except for the fasteners. Three types of fasteners were employed; (1) Lignostone® Transformerwood® laminated densified wood dowels manufactured by Röchling, (2) birch dowels, (3) VGZ steel screws from Rothobaas. Otherwise, the materials utilized for the specimens were birch plywood, Glulam of strength class gl30c and glue. To better understand, a visual representation of the tension test specimen is given in figure 3-2.

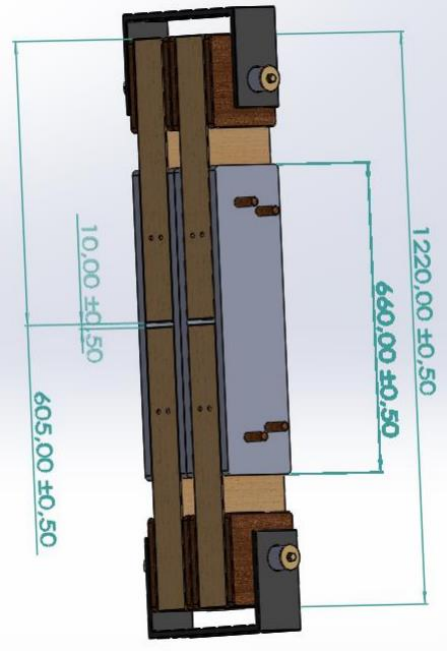

Figure 3- 2 *– Sketch of the tension test specimen with lengths. Light grey and brown plates; Birch plywood, yellow pieces; Glulam, dark grey pieces; steel attachment pieces, brown rods; wood dowels.*

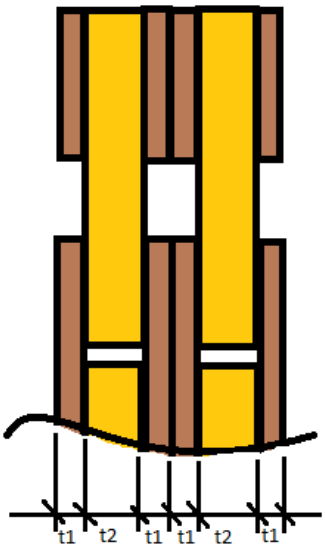

Figure 3- 3 *– Total thickness of the specimen, t=264mm, t1 = 21mm and t2=90mm.*

The total height of the tension test specimen is 1220 mm. This height was decided considering what the test machine allowed. There is also a gap between the end grain of the Glulam pieces of 10 mm. The length of the middle birch plywood plates is 660 mm. The specimen has 4 plywood plates in the middle, one single outer plate on each side, and two plates in the middle. Each plate is 21 mm thick. At each end of the specimens, additional plates of birch plywood are glued to the Glulam pieces, to work as reinforcement of the end so that it would not break in this part. These plywood pieces are described with a detailed drawing in figure 3-4. The specimen also consists of 4 pieces of Glulam, which have a thickness of 90 mm. When layered together, all components make up for a total thickness of 264 mm and four shear planes and a width of 180 mm.

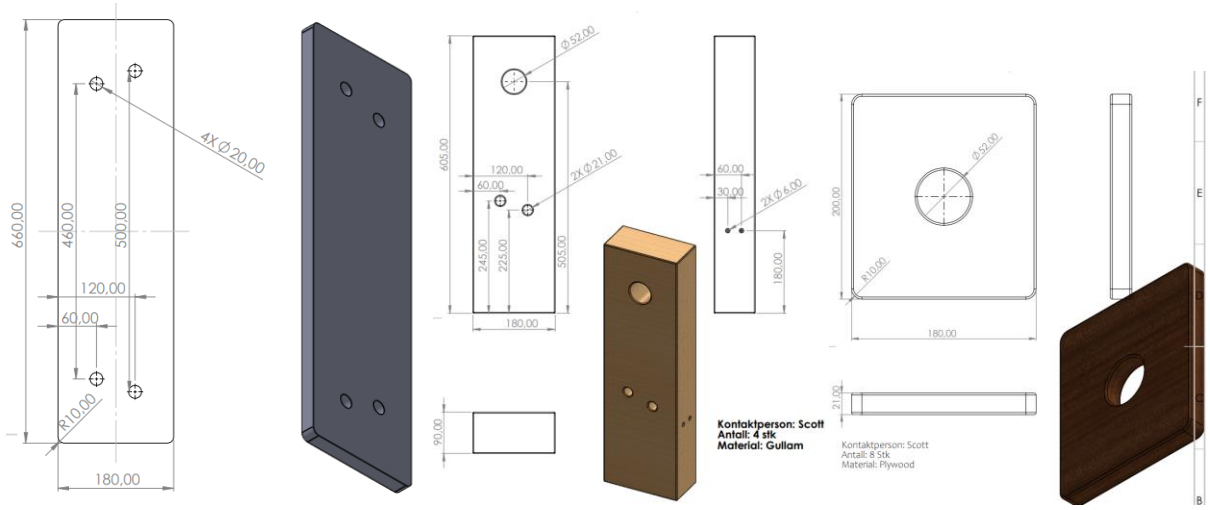

Figure 3- 4 *– Detailed drawings of the middle plywood plates, Glulam pieces and end plywood plates.*

The wood dowels come with a diameter of approximately 20 mm and a length of minimum 300 mm. One of the test groups was constructed with steel screws. The diameter of the dowels is not the same as for the steel screws, but the quantity and placement were the same.

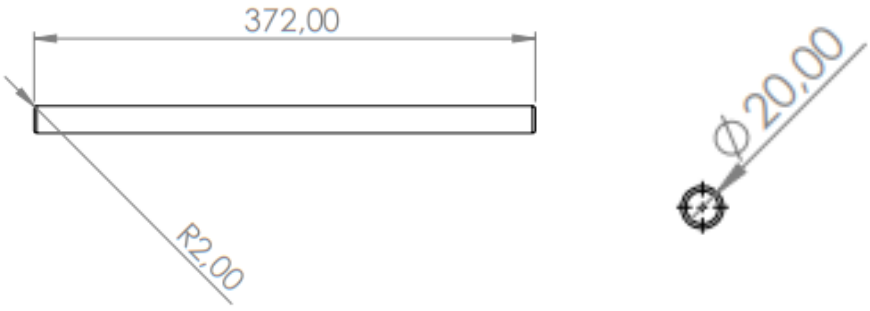

Figure 3- 5 *– Detailed drawing of the wood dowels.*

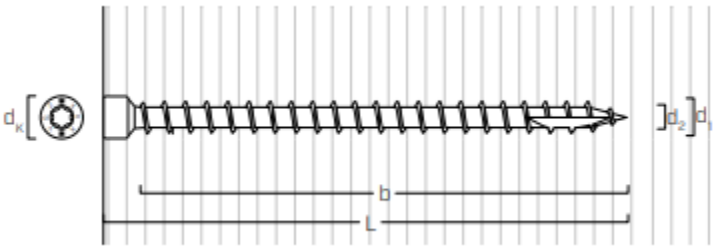

Figure 3- 6 *- Detailed drawing of the VGZ screw from Rothoblaas (Rothoblaas, 2020).*

More specifically the screw from Rothoblaas, used in this experiment, is called VGZ9280. This means that it is 9 mm in diameter and has a length of 280 mm.

Figures 3-2 and 3-4 show 8 predrilled holes in the side of the Glulam pieces, which are meant for steel screws. These screws were inserted to be there as a reinforcement to the end grain of the Glulam pieces. The screws utilized for this were some assorted leftovers from previous experiments in the laboratory. No calculations were done to decide what characteristics these screws should obtain, but they were close to the same kind as the VGZ screws from Rothoblaas.

3.2 Testing Procedure According to NS-ISO 6891:1991

The testing followed the protocol given in the Norwegian Standard NS-ISO 6891:1991, which has been adopted from the International Standard ISO 6891:1991. It provides a reliable method for testing joints made with mechanical fasteners in timber structures. It was developed to

advance the field of load bearing timber structures and has proven to be a well incorporated method utilized in experiments like this. By using this method, information about the strength- and deformation (slip) - characteristics of the specimens can be obtained (NS-ISO 6891:1991, 1991).

Tests of the kind conducted with guidance from NS-ISO 6891:1991 must follow a specific loading process. The testing machine in the laboratory was already programmed to follow this loading process. An estimated force, F_{est}, was all that needed to be calculated ahead. For this research the estimated force was primarily calculated by hand with the analytical models presented in Chapters 2.6 and 2.7. The standard also allows it to be decided based on experience and preliminary testing, which was the case in some of the test groups. The estimated force could also be adjusted if certain criteria are followed (NS-ISO 6891:1991, 1991).

The application of load should follow the pattern given in Figure 3-7. To start off, load should be applied until it reaches 40% of the estimated force. As the test proceeds, it should be held at this force for 30 seconds, and then lowered to 10% of the estimated force, then be held for an additional 30 seconds at this value. After this load can be applied until the test reaches its maximum strength or a deformation (slip) of 15 mm. Before the load reaches 70% of the estimated force, a constant rate of load or slip of $0,2xF_{est}$ per minute, +- 25%, should be maintained. After this the rate can be adjusted and should follow a constant rate of slip. This adjustment should be made in a manner that ensures the test to be done within an additional time of 3 to 5 minutes. This means that the total testing time should be 10 to 15 minutes (NS-ISO 6891:1991, 1991).

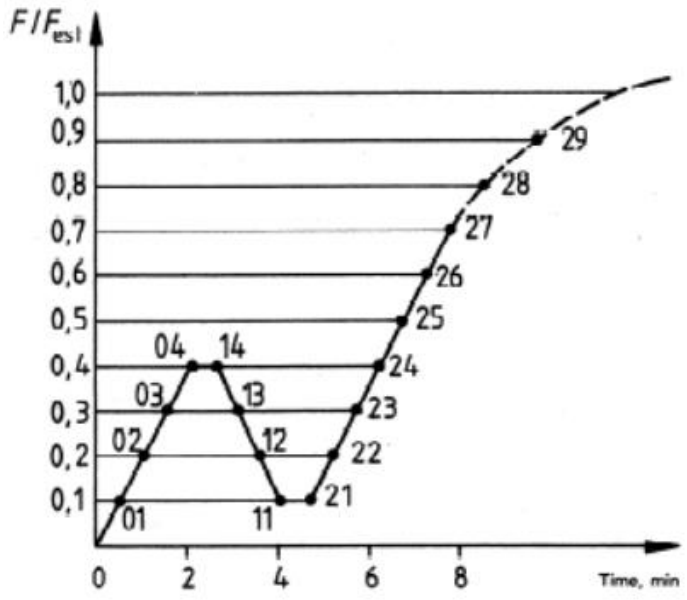

***Figure 3- 7** – "Loading procedure." (NS-ISO 6891:1991, 1991)*

Chapter 8.2 in NS-ISO 6891:1991 also states that the test should be stopped when the ultimate load is reached, or the slip reaches 15 mm (NS-ISO 6891:1991, 1991). However, in the experiments for this thesis the force was rather noted at this limit, and then the test proceeded until ultimate force and deformation was reached.

Additionally, the standard suggests some requirements when it comes to the test environment (NS-ISO 6891:1991, 1991). It is commonly known that the strength characteristics of timber is highly affected by its moisture content. Therefore, the conditions in the environment where the specimens are stored prior to- and while tested, should be ideal. Such conditions were manipulated with the help of an air humidifier which was also able to control the temperature. This ensured that the environment in the lab kept a constant humidity of 60% and a constant temperature of approximately 20°C, which also made sure the moisture content of the wood in each specimen was kept approximately at 12%. The specimens were also kept in the laboratory environment for as long as possible prior to testing to adjust to the right conditions.

3.3 Data Processing in Python and Excel

The measurements from the displacement sensors were not set to be aligned with the measurements from the testing machine. This led to two separate files with results, one from the

machine, and one from the displacement sensors. However, the results from the displacement sensors also plotted the loading and stored the force in a column. So, the set of data that was plotted with the measurements for the displacement sensors, provided all that was necessary, which is the force applied against the displacement of each sensor, #1-4.

Spyder (Python 3.10), was utilized to process the data and produce the results presented by force-displacement graphs in chapter 4. For this purpose, Spyder came to be useful to analyze data as it is designed by and for scientists, engineers, and data analysts. It is written in Python, for Python, and provides features for advanced editing, analysis, debugging, and profiling. It serves many functions of use, but in this case, it was a great tool for exploring the data, and making a code for plotting the graphs this research is pursuing (Spyder, 2023). The script for extraction of the desired data will be provided in Appendix C.

The measurements that were needed to calculate the density and moisture content of the wood dowels, were plotted in Excel. The spreadsheet is presented in Appendix B.

3.4 Test Machine and Test Setup

The machine that was employed for the tension test is called Zwick ZR1200. A visual representation of the machine can be found in Figure 3-8. This machine possesses enough strength to load the tests to failure, as well as saving and plotting the results. It measures both force and displacement at a desired rate.

Figure 3-8 *– The Zwick ZR1200 test machine with the prototype attached in it.*

To restrain the specimens to the machine, the mechanical workshop at NMBU constructed two parts of steel with steel dowels to lock the specimen in and that was strong enough to bear the loading that was applied. Figure 3-9 gives a good perspective of how these pieces look.

Figure 3-9 *– Visual representation of how the specimens is restrained with a fully threaded steel dowel with a diameter of 50mm.*

Even though the Zwick machine was able to measure the displacement of the tests, the values included a slight deformation in the steel attachment pieces in addition to the more desirable values of the deformation of the specimen. It would also include the elongation of every component affected by the loading. The purpose of this research is to get a better look into the deformation of the fasteners. To solve this, four displacement gauges were utilized and placed strategically to each specimen when tested. The devices used for this purpose are manufactured by AEP transducers and are illustrated in Figure 3-10 (AEP transducers, 2020).

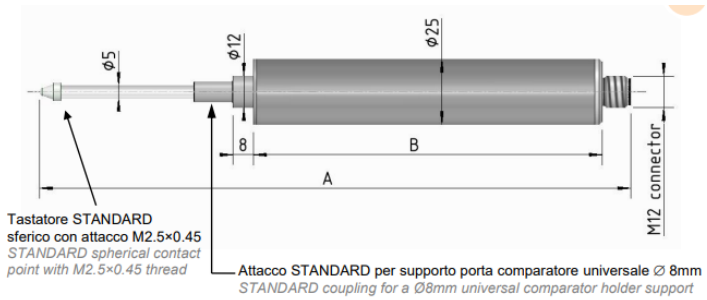

CODE	Displacement	A	B
TLDT5MM	5 mm	120	76
TLDT10MM	10 mm	125	76
TLDT25MM	25 mm	140	76
TLDT50MM	50 mm	223	134
TLDT100MM	100 mm	373	240
TLDT200MM	200 mm	675	434

Figure 3- 10 *– Illustration of the AEP LDT transducer accompanied by a table showcasing the types that was utilized for this experiment, marked with red (AEP transducers, 2020).*

Figure 3-11 shows the configuration of the displacement gauges. Two of the devices were attached so that the slip between the shear planes could be measured. That is, between the plywood plate and the Glulam piece. The remaining two devices were placed so the slip between the end grain of the Glulam pieces could be measured. They were also given a number, #1-4, to be able to mount the transducers similarly in each test. Transducer/sensor #1 and #3 both measured the slip between the Glulam and the outer plywood plates, in approximately the same height as the dowels and screws. Transducer/sensor #2 and #4 both measured the slip between the end grain of the Glulam pieces.

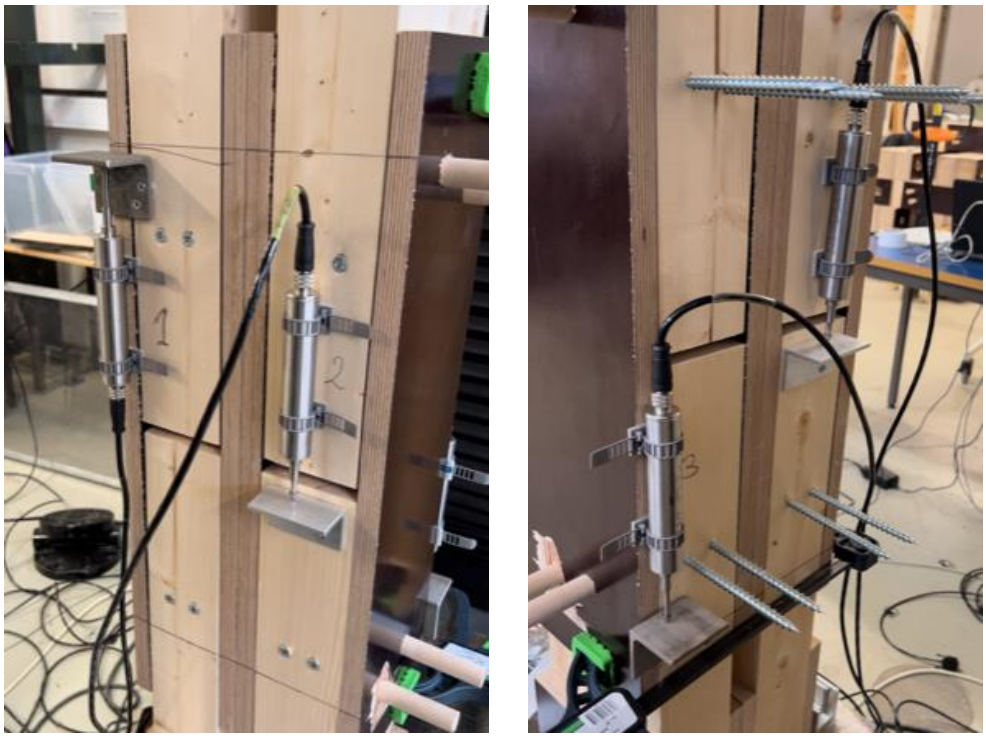

a) b)

Figure 3-11 *– a) and b) visual representation of the placement of the displacement gauges. They are mirrored to ensure that deformations are detected in as many parts of the specimen as possible. They are given a number, #1-4, as you can see in the pictures.*

Tests of this kind, with dowels, tend to make a gap between the shear planes of the specimen when applying a tensile load. Such a phenomenon would have an impact on the capacity of the specimen, as it creates a higher moment and could cause an unintended failure mode for the dowel. To prevent this from happening the specimens were clamped, so that the plywood plates stayed adjacent to the Glulam throughout the whole test. Figure 3-12 shows how the clamps were attached.

Figure 3-12 *– Visual representation of how the clamps is attached to hold the plywood plates adjacent to the Glulam pieces.*

3.5 Test Groups

The tests were divided into three groups, one for each fastener type that was employed in this research. In addition to these three groups, it was decided to do a preliminary test to gather relevant experience for the main testing. Each group, except for the preliminary test, consisted of 5 identical specimens. This means there was a total of 15 tested objects + the "prototype". An overview of the test groups is given in Table 3-1.

Table 3- 1 *– Overview of the test groups, with ID and description.*

Test ID	Description
Prototype	Materials and dimensions as described in chapter 3.1. Fasteners are of the dowel kind, made from beech.
BD-(1-5)	Materials and dimensions as described in chapter 3.1. Fasteners are of the dowel kind, made from birch.
LDW-(1-5)	Materials and dimensions as described in chapter 3.1. Fasteners are of the dowel kind, made from laminated densified wood.
S-(1-5)	Materials and dimensions as described in chapter 3.1, except from the fasteners, which are of the full threaded screw kind. Diameter of the screw is 9mm of the type VGZ9280 from Rothoblaas.

3.6 Density and Moisture Content of the BD- and LDW-Dowels

Even though the density of the birch and the laminated densified wood dowels through earlier studies has been documented, a procedure to calculate this value was conducted to be sure that the materials that was employed were of the same characteristics. Density is given by wight divided by mass as explained in Eq. 3-1.

$$\rho = \frac{m}{V}$$

$where$:

$\rho = density, often\ given\ in\ kg/m^3$

$m = mass$

$V = volume$

Eq. 3- 1 *– Equation for the density of an object.*

Two different approaches were done to measure the density. Birch is lighter than water, which means that Archimedes' principle and weighing could be used to measure the density. However, LDW is heavier than water which made it harder to measure the density with this method. Instead, the volume of each piece of the LDW dowels were measured by hand and then weighed.

The procedure of measuring the density of the birch dowels was to cut off clean pieces from the test. To prevent any unnecessary harm to the piece, a thin saw was used in this process to make the cut as fine as possible. One piece from every birch dowel was extracted, making 20 pieces in total. Each piece was weighed on a fine scale, capable of measuring each gram. Archimedes' principle was then used to measure the volume of the pieces. Knowing the density of water to be 1000 kg/m^3 and the weight of the object, one can calculate the volume of an object by submerging it in water. Eq. 3-2 shows the equation used to get the volume of the birch dowel pieces.

$$m_w = \rho_w * V_o$$

$where$:

$m_w = mass\ of\ water\ displaced\ when\ the\ object\ is\ submerged$

$\rho_w = density\ of\ water$

$V_o = volume\ of\ the\ submerged\ object$

Eq. 3- 2 *– Equation used to find the volume of each piece.*

Moisture content was measured by weight before and after drying. The pieces that were used to evaluate the moisture content were weighed as soon as possible after the tension tests to capture the right moisture content. If the moisture content was evaluated long after the tension tests, the pieces could absorb more moisture, risking that the wrong contents were measured. Eq. 3-3, shows the formula to calculate the moisture content.

$$w_{\%} = \frac{m_i - m_{dry}}{m_i} * 100$$

$where$

$w_{\%} = moisture\ content\ in\ \%$

$m_i = initial\ mass$

$m_{dry} = mass\ after\ drying$

Eq. 3- 3 *– Equation for calculating the moisture content.*

4 Results

This chapter will consist of the results from testing. Mainly, force-displacement graphs will be illustrated to provide a good overview from the tests. There will also be tables linked to the tests with more information about the maximum capacities of each test, results regarding mean moisture content and mean density of the dowels, and other key values that should be reported according to NS-ISO 6891:1991. The results from the measurements of moisture content and density are listed in their own table. Lastly, a table summarizes all values of interest for further investigations.

4.1 Results from the Experimental Investigations of the BD-tests

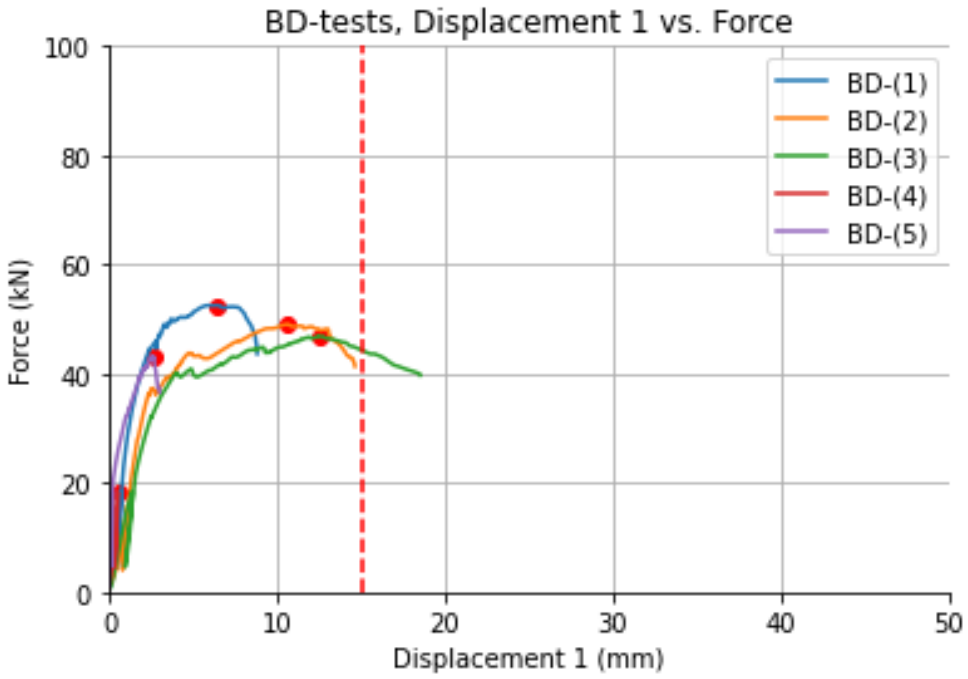

Figure 4- 1 *– Visual representation of the force applied, in kN, vs. the displacement, in mm, measured from sensor #1 from the test with birch dowels. Red dotted line marks 15mm. Red dots mark the maximal force.*

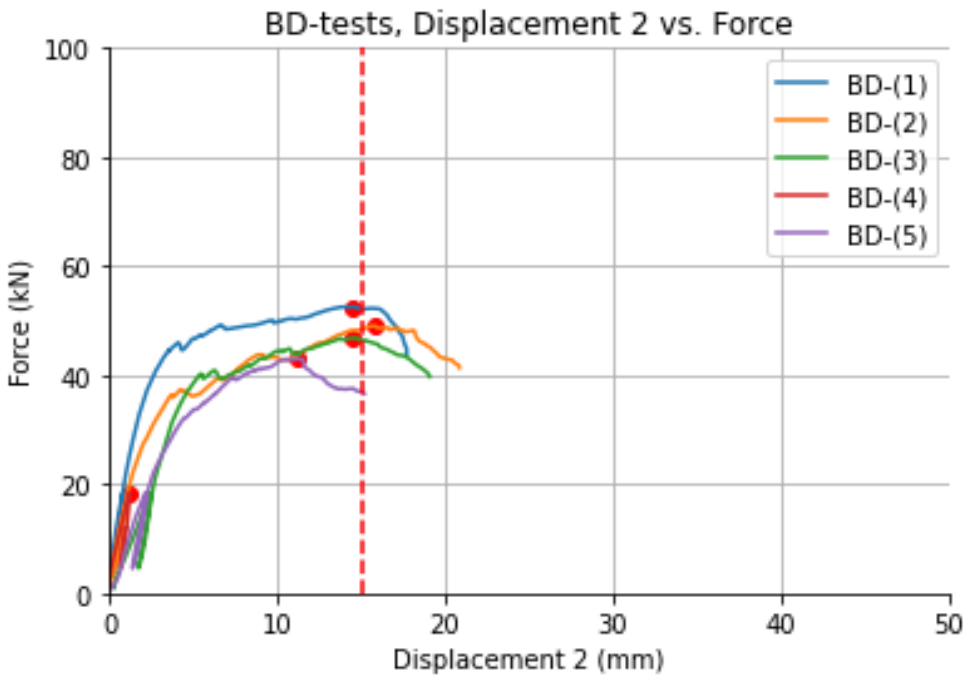

Figure 4- 2 *– Visual representation of the force applied, in kN, vs. the displacement, in mm, measured from sensor #2 from the tests with birch dowels. Red dotted line marks 15mm. Red dots mark the maximal force.*

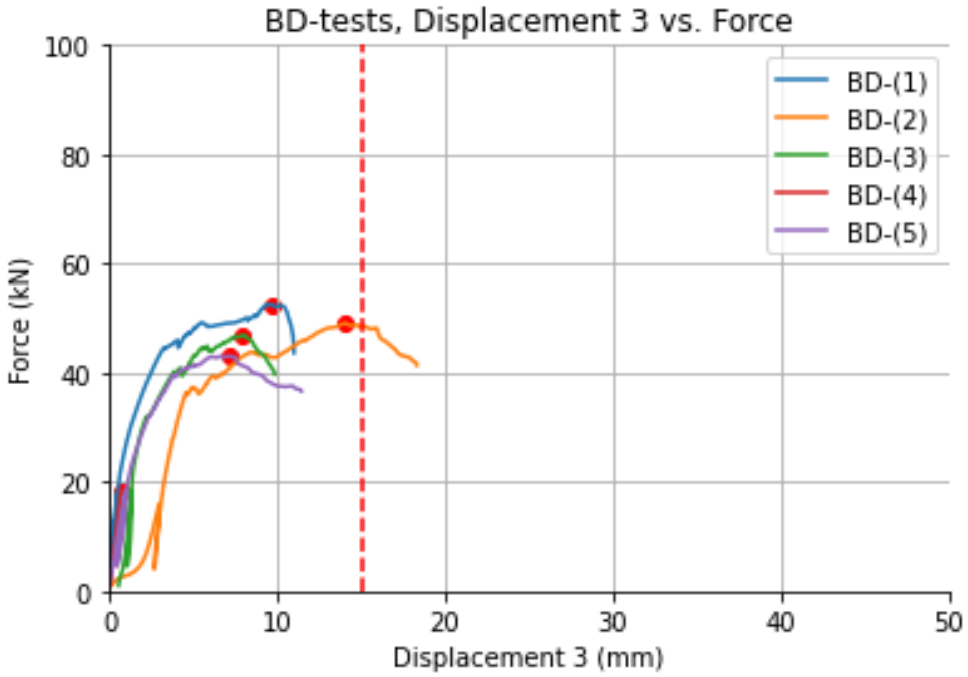

Figure 4- 3 *– Visual representation of the force, in kN, applied vs. the displacement, in mm, measured from sensor #3 from the test with birch dowels. Red dotted line marks 15mm. Red dots mark the maximal force.*

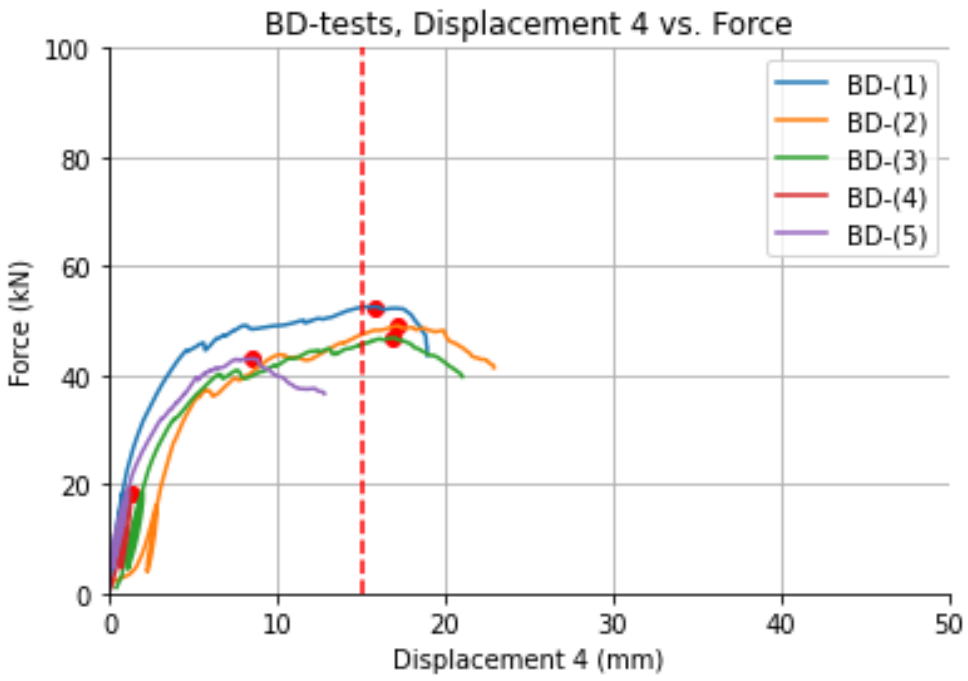

Figure 4- 4 *– Visual representation of the force, in kN, applied vs. the displacement, in mm, measured from sensor #4 from the test with birch dowels. Red dotted line marks 15mm. Red dots mark the maximal force.*

Table 4- 1 *– Overview of specific numbers and info linked to the tests done with birch dowels.*

	BD-(1)	BD-(2)	BD-(3)	BD-(4)	BD-(5)	**Mean Values**
$F_{max,BD}$ $[kN]$	52.54	49.06	46.89	51.86	43.09	48.69
$F_{est,BD}$ $[kN]$	46	40	46	46	46	
$\delta_{1,max\,force}$ $[mm]$	6.35	10.62	12.50	0.52	2.63	6.52
$\delta_{2,max\,force}$ $[mm]$	14.50	15.77	14.49	1.20	11.25	11.44
$\delta_{3,max\,force}$ $[mm]$	9.64	14.09	7.95	0.73	7.15	7.92
$\delta_{4,max\,force}$ $[mm]$	15.82	17.18	16.80	1.29	8.49	11.92
$F_{1,15mm}$ $[kN]$	-	42.73	44.98	-	-	43.85
$F_{2,15mm}$ $[kN]$	52.54	48.26	46.87	-	37.58	46.31
$F_{3,15mm}$ $[kN]$	-	48.68	-	-	-	48.68
$F_{4,15mm}$ $[kN]$	52.07	48.60	45.02	-	-	48.60
$\delta_{1,u}$ $[mm]$	8.82	14.64	18.53	-	3.02	11.25
$\delta_{2,u}$ $[mm]$	17.71	20.85	19.08	-	15.19	18.21
$\delta_{3,u}$ $[mm]$	11.01	18.31	9.86	-	11.45	12.66
$\delta_{4,u}$ $[mm]$	18.93	22.91	21.02	-	12.82	18.92
Failure mode	Shear in the dowel	Shear in the dowel	Shear in the dowel	Shear in the dowel	Shear in the dowel	
$\rho_{mean,BD}$ $[kg/m^3]$	659.8					
$w_{mean,BD}$ [%]	9.9					

Note:

$F_{max,BD}$ ~ ***maximum force experienced during testing***

$F_{est,BD}$ ~ ***estimated force that was set in the testing software***

$\delta_{[\dots],max\,force}$ ~ ***displacement at maximum force***

$\delta_{[\dots],u}$ $[mm]$ ~ ***ultimate displacement***

$F_{[\dots],15mm}$ ~ ***force at 15mm displacement***

$\rho_{mean,BD}$ $[kg/m^3]$ ~ ***mean density for the birch dowels***

$w_{mean,BD}$ [%] ~ ***mean moisture content for the birch dowels***

4.2 Results from the Experimental Investigations of the LDW-tests

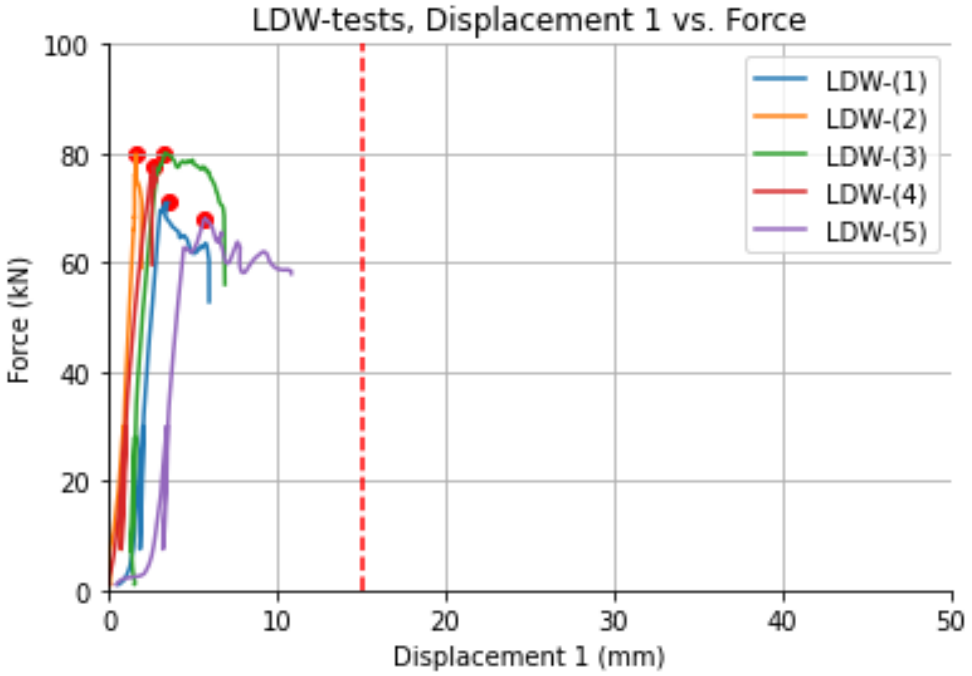

Figure 4- 5 *– Visual representation of the force applied, in kN, vs. the displacement, in mm, measured from sensor #1 from the tests with laminated densified wood dowels. Red dotted line marks 15mm. Red dots mark the maximal force.*

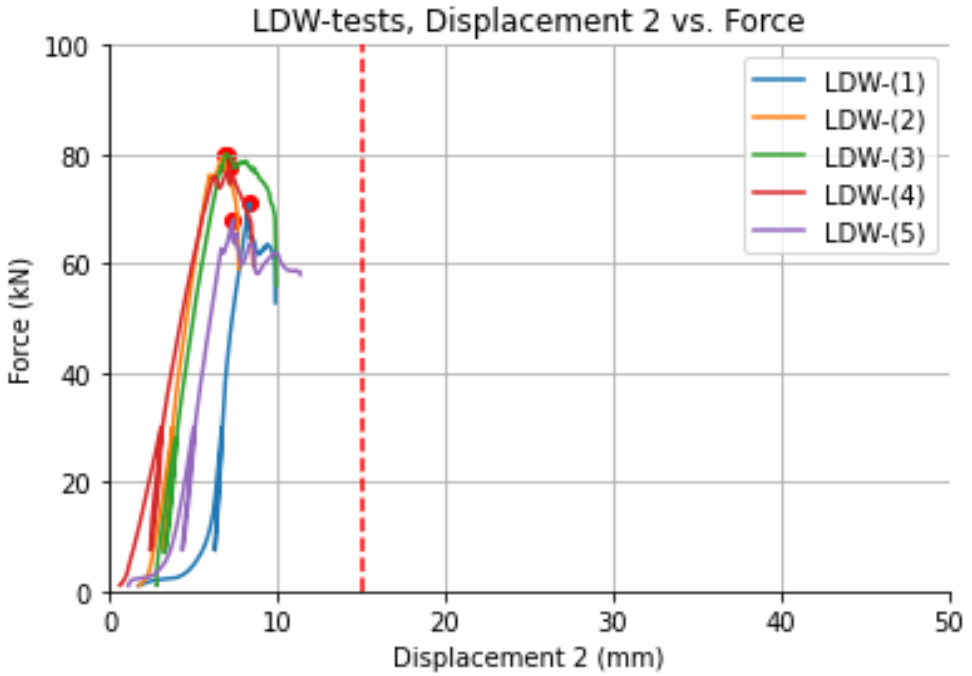

Figure 4- 6 *– Visual representation of the force applied, in kN, vs. the displacement, in mm, measured from sensor #2 from the tests with laminated densified wood dowels. Red dotted line marks 15mm. Red dots mark the maximal force.*

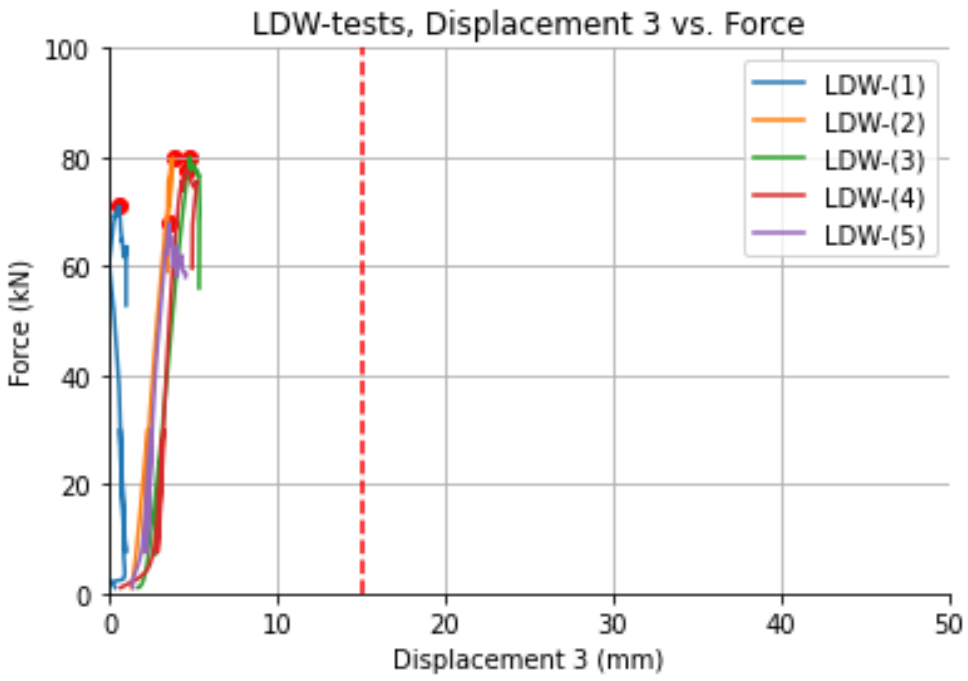

Figure 4- 7 *– Visual representation of the force applied, in kN, vs. the displacement, in mm, measured from sensor #3 from the tests with laminated densified wood dowels. Red dotted line marks 15mm. Red dots mark the maximal force.*

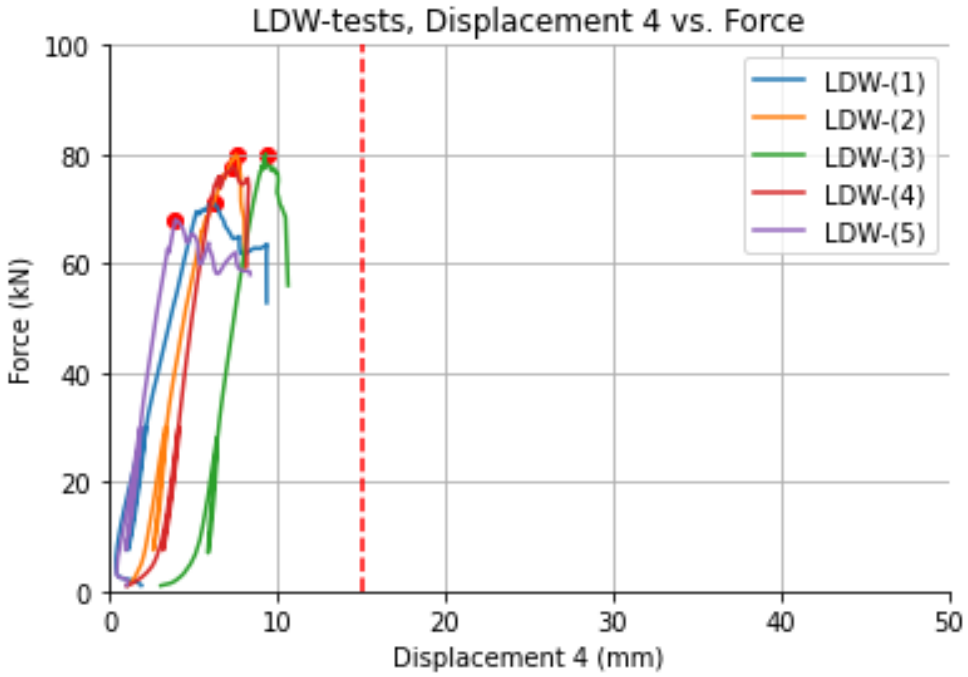

Figure 4- 8 *– Visual representation of the force applied, in kN, vs. the displacement, in mm, measured from sensor #4 from the tests with laminated densified wood dowels. Red dotted line marks 15mm. Red dots mark the maximal force.*

***Table 4- 2** – Overview of specific numbers and info linked to the tests done with LDW dowels.*

	LDW-(1)	LDW-(2)	LDW-(3)	LDW-(4)	LDW-(5)	**Mean Values**
$F_{max,LDW}$ $[kN]$	71.06	79.95	80.07	77.74	68.04	75.37
$F_{est,LDW}$ $[kN]$	75	75	70	75	75	-
$\delta_{1,max\,force}$ $[mm]$	3.52	1.63	3.34	2.68	5.71	3.38
$\delta_{2,max\,force}$ $[mm]$	8.38	6.89	6.93	7.20	7.38	7.36
$\delta_{3,max\,force}$ $[mm]$	0.57	3.80	4.79	4.58	3.57	3.46
$\delta_{4,max\,force}$ $[mm]$	6.21	7.55	9.33	7.35	3.94	6.88
$F_{1,15mm}$ $[kN]$	-	-	-	-	-	-
$F_{2,15mm}$ $[kN]$	-	-	-	-	-	-
$F_{3,15mm}$ $[kN]$	-	-	-	-	-	-
$F_{4,15mm}$ $[kN]$	-	-	-	-	-	-
$\delta_{1,u}$ $[mm]$	5.95	1.96	6.91	2.58	10.85	5.65
$\delta_{2,u}$ $[mm]$	9.90	7.71	9.95	8.60	11.38	9.51
$\delta_{3,u}$ $[mm]$	1.01	3.49	5.36	4.95	4.55	3.87
$\delta_{4,u}$ $[mm]$	9.38	8.08	10.65	8.19	8.40	9.94
Failure mode	-	-	-	-	-	
$\rho_{mean,LDW}$ $[kg/m^3]$				1344.0		
$w_{mean,LDW}$ [%]				3.0		

Note:

$F_{max,LDW}$ ~ ***maximum force experienced during testing***

$F_{est,LDW}$ ~ ***estimated force that was set in the testing software***

$\delta_{[...],max\,force}$ ~ ***displacement at maximum force***

$\delta_{[...],u}$ $[mm]$ ~ ***ultimate displacement***

$F_{[...],15mm}$ ~ ***force at 15mm displacement***

$\rho_{mean,LDW}$ $[kg/m^3]$ ~ ***mean density for the LDW dowels***

$w_{mean,LDW}$ [%] ~ ***mean moisture content for the LDW dowels***

4.3 Results from the Experimental Investigations of the S-tests

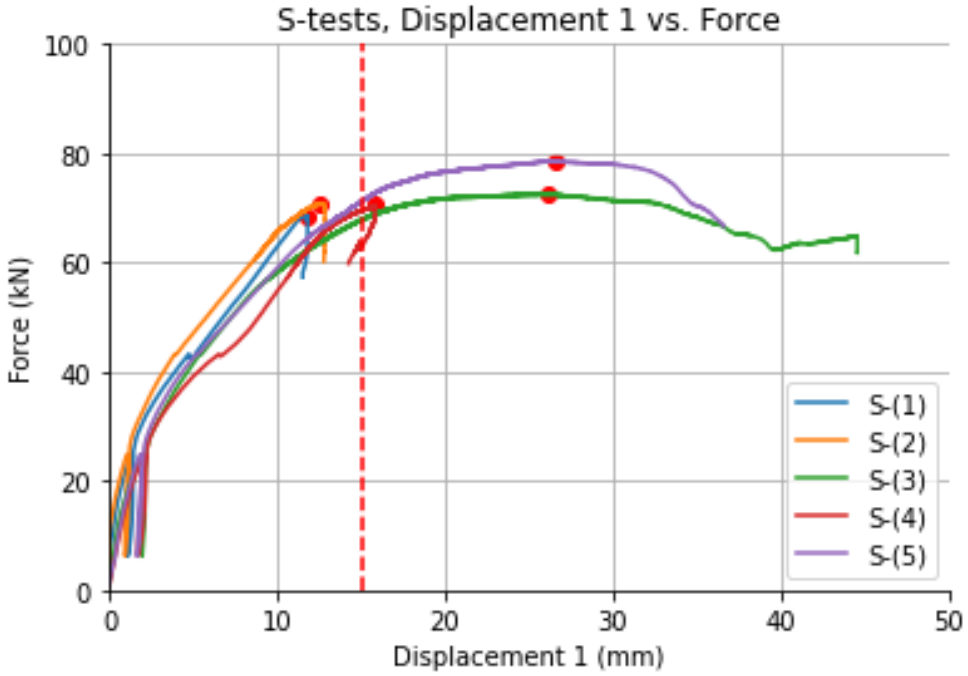

Figure 4- 9 *- Visual representation of the force applied, in kN, vs. the displacement, in mm, measured from sensor #1 from the tests with steel screws. Red dotted line marks 15mm. Red dots mark the maximal force.*

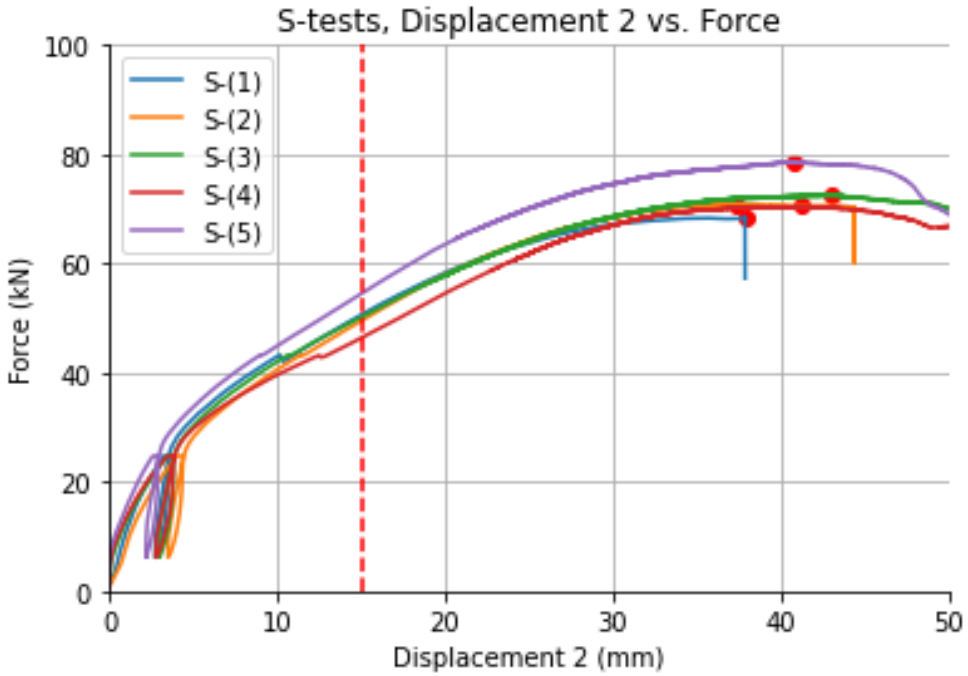

Figure 4- 10 *– Visual representation of the force applied, in kN, vs. the displacement, in mm, measured from sensor #2 from the tests with steel screws. Red dotted line marks 15mm. Red dots mark the maximal force.*

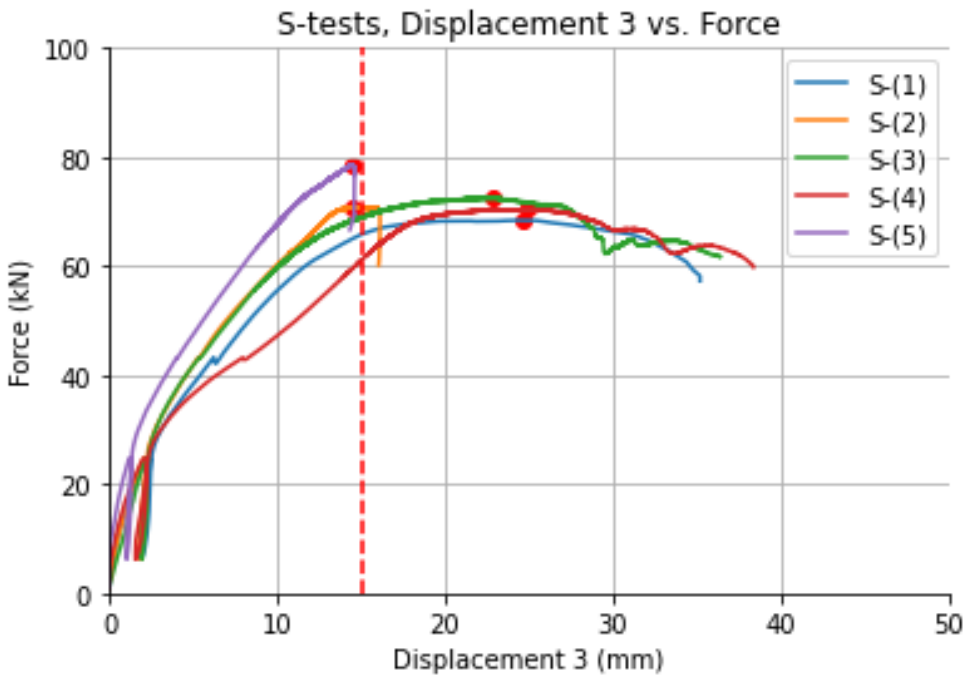

Figure 4- 11 *– Visual representation of the force applied, in kN, vs. the displacement, in mm, measured from sensor #3 from the tests with steel screws. Red dotted line marks 15mm. Red dots mark the maximal force.*

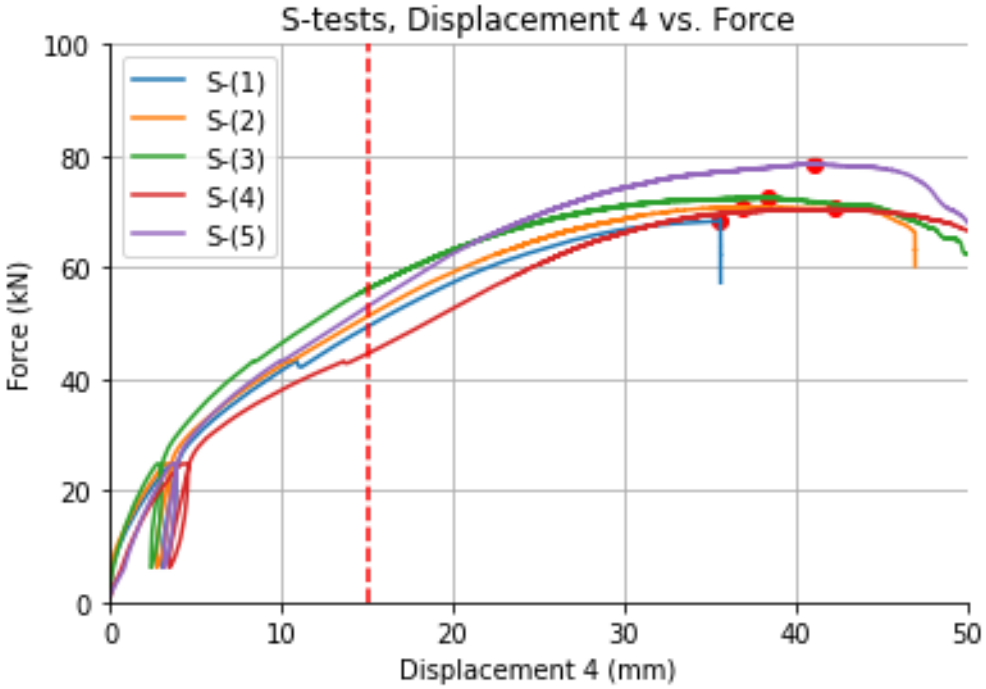

Figure 4- 12 *– Visual representation of the force applied, in kN, vs. the displacement, in mm, measured from sensor #1 from the tests with steel screws. Red dotted line marks 15mm. Red dots mark the maximal force.*

Table 4- 3 *– Overview of specific numbers and info linked to the tests done with steel screws.*

	S-(1)	S-(2)	S-(3)	S-(4)	S-(5)	**Mean values**
$\boldsymbol{F_{max,S}}$ $\boldsymbol{[kN]}$	68.46	70.81	72.58	70.56	78.59	72.20
$\boldsymbol{F_{est,S}}$ $\boldsymbol{[kN]}$	62	62	62	62	62	-
$\boldsymbol{\delta_{1,max\,force}}$ $\boldsymbol{[mm]}$	11.76	12.57	26.11	15.84	26.60	18.58
$\boldsymbol{\delta_{2,max\,force}}$ $\boldsymbol{[mm]}$	37.85	37.27	42.93	41.18	40.83	40.01
$\boldsymbol{\delta_{3,max\,force}}$ $\boldsymbol{[mm]}$	24.62	14.48	22.80	24.88	14.48	20.25
$\boldsymbol{\delta_{4,max\,force}}$ $\boldsymbol{[mm]}$	35.61	36.93	38.34	42.18	41.10	38.83
$\boldsymbol{F_{1,15mm}}$ $\boldsymbol{[kN]}$	-	-	67.15	68.81	70.20	68.72
$\boldsymbol{F_{2,15mm}}$ $\boldsymbol{[kN]}$	49.72	48.58	49.37	45.55	53.52	49.35
$\boldsymbol{F_{3,15mm}}$ $\boldsymbol{[kN]}$	65.06	70.74	68.43	59.55	78.55	68.47
$\boldsymbol{F_{4,15mm}}$ $\boldsymbol{[kN]}$	48.44	50.29	55.28	43.75	51.91	49.93
$\boldsymbol{\delta_{1,u}}$ $\boldsymbol{[mm]}$	11.52	12.79	44.54	14.26	36.59	23.94
$\boldsymbol{\delta_{2,u}}$ $\boldsymbol{[mm]}$	37.86	44.38	51.29	58.30	50.85	48.54
$\boldsymbol{\delta_{3,u}}$ $\boldsymbol{[mm]}$	35.17	16.05	36.39	38.36	14.33	28.06
$\boldsymbol{\delta_{4,u}}$ $\boldsymbol{[mm]}$	35.62	46.96	51.29	59.77	50.44	48.82
Failure mode	-	-	-	-	-	

Note:

$\boldsymbol{F_{max,LDW}}$**~maximum force experienced during testing**

$\boldsymbol{F_{est,LDW}}$**~estimated force that was set in the testing software**

$\boldsymbol{\delta_{[\dots],max\,force}}$**~displacement at maximum force**

$\delta_{[\dots],u}$ $[mm]$~*ultimate displacement*

$\boldsymbol{F_{[\dots],15mm}}$**~force at 15mm displacement**

4.4 Density and Moisture Content Results

Listed below, in Table 4-4, are the results from the measurement of density and moisture content of the wood dowels. A full overview can be found in Appendix B.

Table 4- 4 *– Overview of the measured mean, maximal and minimum densities, and moisture contents for the wood dowels from each test.*

	Density, ρ [kg/m^3]			Moisture content, w [%]		
	Mean	Max.	Min.	Mean	Max.	Min.
BD-(1)	657.0	687.3	624.2	-	-	-
BD-(2)	667.1	695.7	619.9	-	-	-
BD-(3)	660.1	724.8	630.1	9.9	10.1	9.6
BD-(4)	657.0	693.3	615.7	-	-	-
BD-(5)	657.7	710.1	615.8	-	-	-
LDW-(1)	1327.3	1358.6	1296.9	3.3	4.0	2.7
LDW-(2)	1358.8	1364.2	1347.5	2.7	3.0	2.4
LDW-(3)	1353.8	1369.8	1347.7	2.9	3.6	2.6
LDW-(4)	1348.4	1372.7	1334.1	3.1	3.4	2.6
LDW-(5)	1331.7	1358.6	1301.7	3.2	3.8	2.8

4.5 Summary Results According to NS-ISO 6891:1991

Table 4- 5 *– Summary of the main results of interest. It follows the rules provided in NS-ISO 6891:1991.*

		LDW	BD	S
F_{est}	[kN]	81.47	41.40	62.76
$F_{max,m}$	[kN]	75.37	48.69	72.20
$\delta_{max,m}$	[mm]	4.76	11.96	15.00
ρ_m	[kg/m^3]	1344.00	659.80	-
w_m	[%]	3.00	9.90	-

Note:

F_{est} – estimated force based on calculations.

$F_{max,m}$ – mean maximal force from experiments

$\delta_{max,m}$ – mean maximal deformation according to NS-ISO 6891 :1991, accounting for sensors #1 and #3

ρ_m – mean density

w_m – mean moisture content

5 Discussion

In the following chapter the results will be evaluated by comparing the performance of test groups to each other, and the research questions, RQ- 1 and 2, presented headmost of this paper will be debated. Furthermore, implications and limitations acquainted during the experimental study will be elaborated, and proposals for further work within this topic will be presented.

5.1 Evaluation of the Overall Force-Deformation Behavior of the Tension Tests

The behavior of the connections can be discussed by the results presented in Chapter 4. When comparing the overall strength of the test groups to each other, it was the tests with LDW dowels that endured the highest load. The absolute maximal strength was achieved in LDW-(3), which endured a load of 80.066 kN. That is approximately 27.5 kN more than the maximal strength achieved among the BD-tests (BD-(1)), and approximately 1.9 kN more than for the S-tests (S-(5)). The minimum strength amongst the LDW-tests was found to be 68.035 kN, 43.088 kN for the BD-tests and 68.464 kN for the S-tests. The mean strength of the LDW-tests was 75.370 kN with an SD (standard deviation) of 5.50, whereas for the BD-tests it was a mean value of 48,687 kN with an SD of 3,86 and a mean value of 72.198 kN with a SD of 3.86 for the S-tests. The standard deviations reflect the range of the results, where the highest range is found in the LDW-tests. It is hard to tell exactly why the deviation is higher for the LDW tests, but what might cause deviation within the groups can be debated when evaluating the measured moisture content and density of the wood dowels.

When investigating the measured density and moisture content of the LDW-tests a trend affecting the strength of the connections is observed. Whether the influence of density and moisture content is the only factor affecting the strength is unclear. However, these are the only experimental measurements that can be directly linked to the tension tests. As presented earlier in this thesis, the shear behavior of the wood dowel can be significantly influenced by the density relative to the force-displacement performance and failure mode of the connection (Sandoli, et al., 2023). Furthermore, it is recorded in the results, that with increasing density and decreasing

moisture content, the strength of the connection increases. When the strongest specimens are compared to the weakest, the accompanying densities and moisture contents are found to have a markable difference to each other. This might be applicable for the BD-tests as well, but among these tests the results do not deviate from each other as much, so to assess this trend for the BD-dowels is considered not to be feasible. Table 5-1 presents an overview of the trend. It should be emphasized that other factors might also influence the deviating results for the LDW-tests.

Table 5- 1 *– Overview of a trending increasement in strength with the increasement of density and decreasing in moisture content for the LDW-dowels.*

		Strength [kN]	Mean ρ [kg/m^3]	Max ρ [kg/m^3]	Min ρ [kg/m^3]	Mean w [%]	Max w [%]	Min w [%]
Weak	LDW-(5)	68	1332	1359	1302	3.2	3.8	2.8
	LDW-(1)	71	1327	1359	1297	3.3	4.0	2.7
Strong	LDW-(4)	77	1348	1372	1334	3.1	3.4	2.6
	LDW-(2)	79	1358	1364	1348	2.7	3.0	2.4
	LDW-(3)	80	1353	1369	1348	2.9	3.6	2.6

When it comes to the deformation recorded through the experiments, the observed results are diverse. The highest deformations occur in the tests with steel screws, and the least deformations occur in the tests with laminated densified wood. Accounting for the displacements measured from sensor #1 and #3, the LDW-tests showed a mean ultimate value of 4.76 mm, the S-tests a mean value of 26.00 mm and the BD-tests a mean value of 11.96 mm. For sensors #2 and #4 the mean value for the ultimate displacement from the LDW-tests was 9.73 mm, 48.68 mm for the S-tests and 18.56 mm for the BD-tests. There is a significant difference between the tests when it comes to the displacement. However, in real life you can only allow so much deformation. As presented in Chapter 3, the testing procedure should be stopped at a deformation/slip of 15mm according to NS-ISO 6891:1991 (1991). The LDW-tests never exceeded this limit, whereas some of the BD-tests and all the S-tests did. For this reason, it is applicable to compare the results at a maximal displacement of 15 mm. This means that the mean ultimate displacement from sensors #1 and #3 is unchanged for the LDW- and BD-tests, and 15mm for the S-tests. The mean ultimate displacement for sensors #2 and #4 is unchanged for the LDW-tests, and 15mm for the

BD- and S-tests. When accounting for the demands given in NS-ISO 6891:1991 (1991), the range of the displacement is heavily reduced for the S-tests. For evaluating whether laminated densified wood is suitable to use as dowels in a multiple shear connection with gusset plates, the 15mm limit could mean that it is more comparable to steel and birch in terms of ductility. It should be emphasized that the most valuable results in terms of deformation is the one measured from sensor #1 and #3 as they measure the slip-ratio more directly to the dowels.

5.2 Discussion of the Ductility Ratio

Laminated densified wood dowels are undoubtedly made of a material with high strength capacities and hardness. Results show that it possesses higher strengths than the birch dowels, and comparable strengths to the steel screws. One of the aspects where the LDW dowels differ from the other fastener types is the ability to withstand deformations. By evaluating the results, it is reasonable to assume that the LDW-tests show the least ductile behavior, as it withstood the least deformation. However, no good ways were found to calculate the ductility ratio, as the results were unable provide applicable values for estimating the yielding points. For this research the only indications in terms of the ductility can be evaluated by comparing the graphs to each other. Otherwise, it is suggested that evaluation of ductility ratios of timber-to-timber connections with laminated densified wood dowels should be properly investigated in future work.

5.3 Failure modes

To better evaluate the failure modes, pictures were taken of the dowels from each specimen from the LDW- and BD-tests. Figures 5-2 and 5-3 show these pictures, illustrating their deflected shape. Unfortunately, the process of extracting the screws for further investigations and comparison to the wood dowel tests, was more complicated than expected. However, it is reasonable to assume that failure mode (III_s) or (IV) was developed in these tests as the deformations that was recorded was high. Additionally, the analytical calculations conducted in accordance with NS-ISO 6891:1991 also predicted these failure modes. To substantiate this, Figure 5-1 illustrates the behavior of the deformation by reviewing lines drawn prior and after

testing S-(1). This shows large displacements in every shear plane, suggesting that both embedment in the members and plastic hinges occurred. Another aspect substantiating this is that the fastener was slender, causing it to have less contact area where the stresses are applied, and thus making it more exposed for embedment in the base material.

(a) (b)

Figure 5- 1 *– Illustration of lines drawn on S-(1); (a) prior to testing; (b) after testing.*

After evaluation of the extracted dowels from the BD-tests, the signs of a shear dominated failure were apparent. Primarily, this can be confirmed by the analytical calculations, which predict that the dowels shear capacity will be decisive for the capacity of the connection. Secondly, the ruptures illustrated in Figure 5-2 do not reflect any of the failure modes (I_s), (II_m), (III_s) or (IV), presented in Chapter 2.7.3.

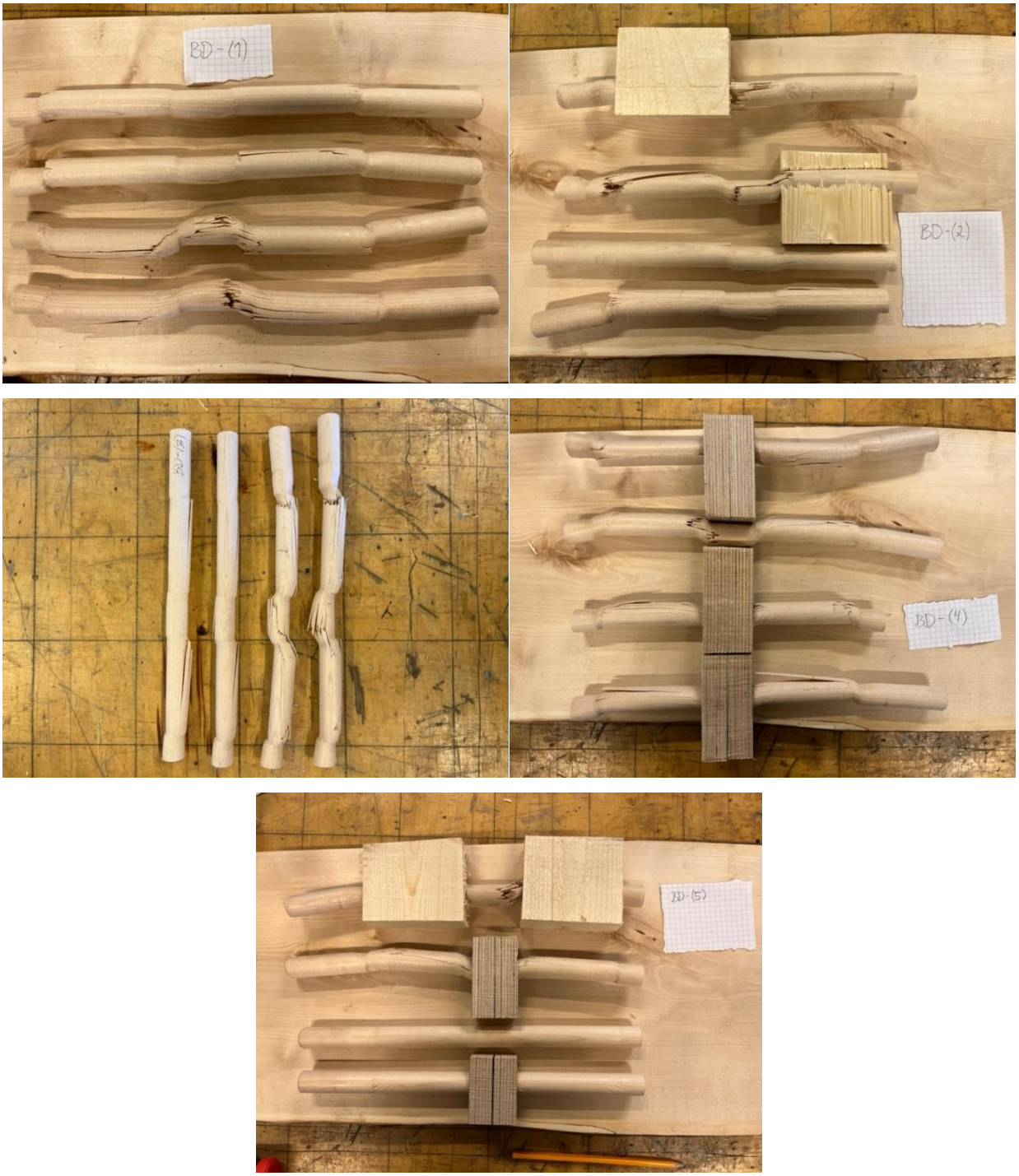

Figure 5- 2 *– Illustrations of the extracted dowels from the BD-tests.*

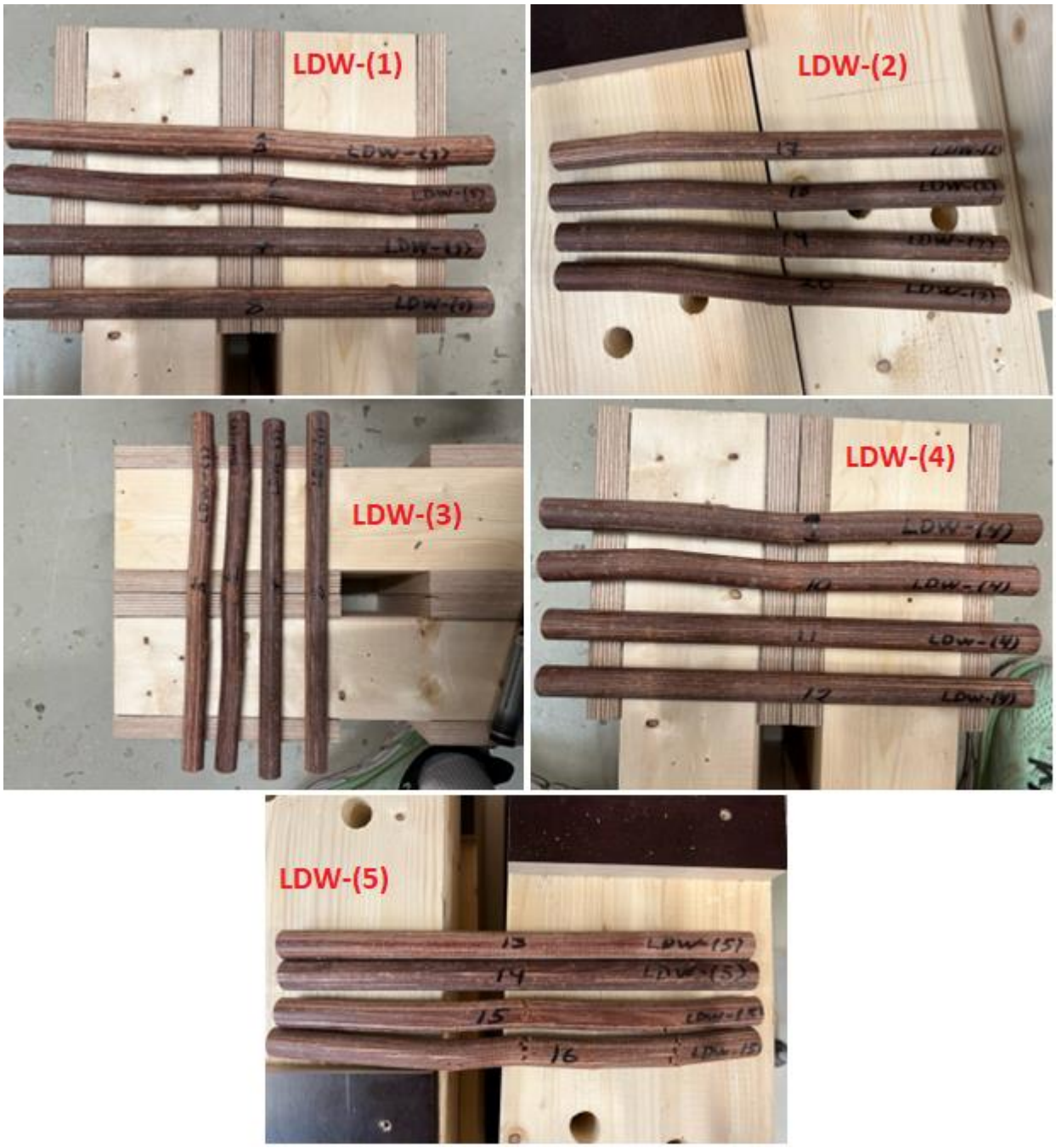

Figure 5- 3 *– Illustrations of the dowels extracted from the LDW-tests.*

In comparison, when evaluating the extracted dowels from the LDW-tests, the signs of a similar failure mode as the BD-tests were not as apparent. According to the analytical calculations, it should in this case, similarly to the BD-tests, be the shear capacity of the dowels that is decisive for the capacity of the LDW-tests. However, one major difference is that it shows a significantly less deflected shape than the birch dowels, which is also reflected when comparing the

deformation results in Chapters 4.1 and 4.2. Additionally, even though it is hard to assess, the deflected shape does not necessarily represent shear failure. When it comes to the evaluation of the failure mode of the LDW-tests, further investigations are needed. The only aspect that is clear in this case is that the analytical model used to calculate the strength capacity of the LDW-tests implies that the governing failure mode is the shear capacity of the dowel.

5.4 Experimental Results Compared to Analytical Models

Table 5-2 reviews the utilization rate between the analytical model used to calculate the strength of the connection. It includes both the maximal forces detected and the forces detected at a displacement of 15mm in accordance with the testing procedure given in (NS-ISO 6891:1991, 1991).

Table 5- 2 *– Overview of utilization rates between the estimated force from analytical calculations and measured forces from the experiments.*

	BD	**LDW**	**S**
F_{est} [kN]	41.4	81.5	62.8
$F_{max,m}$ [kN]	48.7	75.4	72.2
$F_{est}/F_{max,m}$ [%]	85	108	87
$F_{15mm,1,3,m}$ [kN]	-	-	68.6
$F_{est}/F_{15mm,1,3,m}$ [%]	-	-	92

Note:

F_{est} – estimated force from analytical calculations

$F_{max,m}$ – mean maximal force from experiments

$F_{15mm,1,3,m}$ – mean force at 15mm displacement for displacement gauges #1 and #3 from experiments

$F_{15mm,2,4,m}$ – mean force at 15mm displacement for displacement gauges #2 and #4 from experiments

For this research, it is decided to not focus on the displacement measured from displacement sensors #2 and #4 as they include too many additional slip ratios. The displacements measured from sensors #1 and #3 are more representable for the slip ratios of the connection. In the light of this, it has been calculated an additional force in accordance with the rules provided in NS-IS 6891:1991. This force represents the mean force at the 15 mm displacement limit.

To evaluate whether the analytical models presented in this paper are suitable for calculating the strength of the connection, some aspects need to be addressed. If the results are directly evaluated based on the values listed in Table 5-2, it would be justifiable to assume that the analytical models used in this thesis are applicable for calculating the strength of a timber-to-timber multiple shear connection with wood dowels. The utilization rates show that the estimated force is 108 % of the mean maximal force recorded in the LDW-tests. Optimally, it is preferred that this rate is as close to 100% as possible. It should also be mentioned that the rate is rather desired to be less than 100% than greater when designing a structure, as a precautionary measure to make sure that the load does not exceed the capacity. On the other hand, a deviation of 8% is less than the deviation for the BD- and S-tests. The Utilization rate for the BD-tests was 85% and 87% for the S-tests. Accounting for the results presented in Table 4-5, the deformation in the LDW-tests and BD-tests never exceeded the 15 mm limit, so $F_{max,m}$ is applicable for calculating the utilization rate. As for the S-tests, the slip exceeds 15 mm, so $F_{15mm,1,3,m}$ should be used for calculating the utilization rate. This means that the utilization rate is 92% for the S-tests. The fact that the utilization rates are on the precautionary side for the BD- and S-tests, and not the LDW-tests, raises a question of whether the analytical model used to estimate the shear strength of the connection is in need for modifications when it comes to employing LDW dowels.

Considering that the utilization rates are not that far off, it could be presumed that the shear calculations are right. However, this means the calculations conducted according to the modified EYM, presented by Sandoli, et al. (2023), do not have any comparability to the experimental results from the LDW- or the BD-tests. The modified EYM resulted in a F_{est} of 63.7 kN for the BD-tests and 123.2 kN for the LDW-tests. Neither of the values reflect the experimental results or the deflected shape of the dowels. The analytical calculations are presented step by step in Appendix A.

5.5 Implications and Limitations in the Experiment

Through this study implications have appeared along the way. Some of which have caused limitations for the work.

Among the aspects of designing the test specimens and test set up, the configuration of the displacement sensors was one of the most debatable issues. In the aftermath, other configurations may have worked better. It was decided focus more on displacement sensors #1 and #3, as these measured the displacement more direct to the fasteners than displacement sensors #2 and #4. As previously explained, measurements from displacement sensors #2 and #4, includes the elongation of the plywood plate. It is hard to evaluate to what degree this elongation was large or small. Either way, it was unclear how comparable displacement #1 and #3 was to displacement #2 and #4.

One of the main aspects of designing the specimens was to make them on the more massive side, so that the dimensions of the connection would be realistic to a real-life timber-to-timber connections with wood dowels. The size of the specimens made it essential to get hold of the right tools to make it as symmetrical and aligned as possible. Even though the specimens were constructed at a proper workshop, they had slight misalignments. In what degree this affected the results is unclear, but it is necessary to consider it as a source of error. Noticeable variations in the results within the test groups are recorded, especially when comparing the four measured deformations of each test. The reason for this could be because of misalignments and unsymmetric details in the specimens. Regardless, it is evident that symmetry and proper alignments are maintained during and after the construction.

The moisture content that was measured slightly deviated from the optimal values, and the values that the lab environment should be able to keep it at. It is a possibility that the air conditioning was mis calibrated as the facilities was new. However, it could have been that the measurements should have been done more thoroughly, or that the specimens could have been held for a longer time in the lab environment.

Deformation in the steel pieces, meant for restraining the specimens during testing, was not accounted for. Even though improvements were made after testing the prototype, an undesirable deformation occurred in these pieces while testing. The consequences of this were not severe, as deformation was recorded separately, but it is something to be aware of for tests like this.

The credibility of the results from the displacement sensors is somewhat questionable. They are very sensible to errors. For instance, if the sensor slipped out of position, it was affecting the results for that specific sensor, which occasionally happened. Another case, which is the reason

for no deformations listed for BD-(4), was that the computer linked to the transducers stopped recording while testing due to full storage on the computer. One last case occurred during the first two S-tests, S-(1) and S-(2), where most of the displacement sensors reached their maximum potential, meaning that deformation was not registered after this. These are some of the issues that have been encountered, however, the results presented should be sufficient for assessing the aims of the thesis.

5.6 Further work

Overall, the experimental process was time consuming. It was desirable to conduct other experiments as well to better understand the behavior of the connection. Now, that will be of interest for further work.

Embedment strength, bending capacity and shear capacity of laminated densified wood dowels should be further investigated and compared to other materials. This would be helpful in the pursuance of developing good design models and understanding the complexity of timber-to-timber connections with LDW-dowels. It is also suggested that this research is extended with further investigation of different types of pure wood connections. A potential test setup that can be adopted for further investigations is presented in an article by Mehra, et al. (2022).

The ductility of a pure wood connection with laminated densified wood dowels should also be further investigated. LDW has proved itself to be a potential substitute for steel in multiple shear connections when strength is the only parameter, but this research falls short in evaluating whether the ductility ratio is within an acceptable range. It should be possible to manipulate the ductility by for instance adjusting slenderness- and density-ratios, the dowel diameter, and the number of dowels.

Lastly, results from numerical- and experimental investigations can be compiled and processed to form an optimized analytical model for designing purposes of pure wood connections with dowels of laminated densified wood.

6 Conclusion

The current study aimed to investigate the behavior of the material known as “laminated densified wood” employed as dowels in a timber-to-timber multiple shear connection. Relevant theory and methods were presented to form a framework for the experiments conducted and further evaluation of these. Detailing and construction of a tension test set-up was conducted. To establish comparable results, specimens with other fastener types were also tested, i.e., birch dowels and steel screws.

The LDW-tests showed a substantially higher capacity than the BD-tests, and similar capacity to the S-tests. With strength as the only parameter, laminated densified wood poses as a promising material for fasteners. In contrast, the LDW-tests endured the least deformation. This raises a concern as to whether laminated densified wood meets the modern-day requirement for structural design of connections with respect to the ductility ratio. It would be beneficial if future research were to focus on the ductility-ratio, as the results in the current study did not uphold this consideration.

Evaluation of the deflected shapes showed a difference between the birch dowels and the LDW-dowels. While the BD-tests showed clear signs of failure due to the shear capacity of the dowels, the deflected shape of the LDW-dowels were vaguer, which made it hard to identify the failure mode.

The applicability of the equation presented by Miller & Schmidt (2004), for calculating the shear capacity of wood dowels, showed promising results. Further research should however investigate whether this equation is applicable for LDW-dowels, or the possibility of modifying it. Adequate results were not achieved to evaluate the applicability of the modified European Yielding Model presented by Sandoli, et al. (2023).

Overall, laminated densified wood dowels have proven to be capable of carrying great loads. It is encouraged to investigate ways of incorporating this as a standardized fastener material in structural pure wood connection designs.

References

AEP transducers, 2020. *https://www.aep.it/en/company/.* [Online]
Available at: https://www.aep.it/wp-content/uploads/2020/02/LDT.R8.pdf
[Accessed 5 July 2023].

ASTM, 2013. *Standard test method for evaluating dowel-bearing strength of wood and wood-based products ASTM D5764-97a.* West Conshohocken: ASTM International.

Blaß, H., Ernst, H. & Werner, H., 1999. *Verbindungen mit Holzstiften. Untersuchungen über die Tragfähigkeit.* s.l.:Bauen mit Holz.

Blaß, H. J. & Sandhaas, C., 2017. *Timber Engineering Principles for Design.* s.l.:KIT Scientific Publishing .

Boruvka, V., Zeidler, A., Holeˇcek, T. & Dudík, R., 2018. Elastic and Strength Properties of Heat-Treated Beech and Birch Wood. *Forests,* Volume 9, p. 18.

Crocetti, R. et al., 2020. *MULTIPLE SHEAR PLANE CONNECTIONS WITH TIMBER BASED GUSSET PLATES.* Santiago, Chile, In Proceedings of the World Conference on Timber Engineering (WCTE).

Edvardsen, K. I. & Ramstad, T. Ø., 2014. *Trehus.* s.l.:SINTEF akademisk forlag.

Forest Product Laboratory, 2010. *Wood handbook—Wood as an engineering material.* Centennial Edition ed. Madison, Wisconsin: U.S. Department of Agriculture, Forest Service, Forest Products Laboratory.

Furuheim, E. F. & Nesse, P. M., 2020. *Beam-Column Connections in Glulam Structures, with Gusset Plates of Birch Plywood and Self-Tapping Screws,* Ås : Norwegian University of Life Science.

Himes, A. & Busby, G., 2020. Wood buildings as a climate solution. *Developments in the Built Environment,* Volume 4, p. 7.

Koskisen Group, 2002. *Handbook of Finnish Plywood.* Järvelä, Finland: Finnish Forest Industries Federation.

Kromoser, B., Braun, M. & Ortner, M., 2021. Construction of All-Wood Trusses with Plywood Nodes and Wooden Pegs: A Strategy towards Resource-Efficient Timber Construction. *Applied Sciences,* Volume 11, p. 17.

Labaran, Y. H., Mathur, V. S. & Farouq, M. M., 2021. The carbon footprint of construction industry: A review of direct and indirect emission. *J Sustain Const Mater Technol,* 6(3), pp. 101-105.

Larsson, G., 2020. Dowel design of the shear plate dowel joint. *Engineering Structures,* Volume 209, p. 10.

Mehra, S. et al., 2022. Experimental investigation of the moment-rotation behaviour of beam-column connections produced using compressed wood connectors. *Construction and Building Materials,* Volume 331, p. 10.

Miller, J. F. & Schmidt, R. J., 2004. *Capacity of Pegged Mortise and Tenon Joints,* Laramie: Department of Civil and Architectural Engineering University of Wyoming.

NS-EN 1995-1-1:2004, 2004. *Eurocode 5: Design of timber structures.* s.l.:Standard Norge.

NS-ISO 6891:1991, 1991. *Timber Structures-Joints Made with Mechanical Fasteners-General Principles for the Determination of Strength and Deformation Characteristics.* 1 ed. s.l.:Standard Norge.

Röchling Industrial , 2023. *https://www.roechling.com.* [Online]
Available at:
https://www.roechling.com/fileadmin/downloads/Roechling_Industrial/Brochures/EN/Lignostone/Folder-Industrial-Transformatoren-final-web-EN2023.pdf
[Accessed 11 July 2023].

Röchling, 2015. *Technishes Datenblatt Lignostone® Transformerwood® Rundstäbe,* s.l.: Röchling.

Rothoblaas, 2020. *https://www.rothoblaas.com/catalogues-rothoblaas.* [Online]
Available at: https://issuu.com/rothoblaas/docs/screws-and-connectors-for-timber-2021-en?mode=embed
[Accessed 5 July 2023].

Sandoli, A., Ceraldi, C. & Prota, A., 2023. Feasibility of Timber Pegged Joints for Seismic Design of Structures. *Journal of Structural Engineering,* 149(5), p. 13.

Smith, I., Asiz, A., Snow, M. & Chui, Y. H., 2006. *Possible Canadian/ISO approach to deriving design values from test data.* Florence, Italy, Interuniversity Consortium for Biotechnology.

Spyder, 2023. *spyder-ide.* [Online]
Available at: https://www.spyder-ide.org/
[Accessed 5 July 2023].

Švajlenka, J. & Kozlovská, M., 2021. *Constructions of buildings based on solid wooden elements.* s.l., IOP Publishing.

Swedish Wood, n.d. *https://www.swedishwood.com/.* [Online]
Available at: https://www.swedishwood.com/building-with-wood/about-glulam/
[Accessed 10 July 2023].

The Engineering ToolBox, 2011. *https://www.engineeringtoolbox.com/.* [Online]
Available at: https://www.engineeringtoolbox.com/timber-mechanical-properties-d_1789.html
[Accessed 11 July 2023].

Appendix A – Analytical Calculations

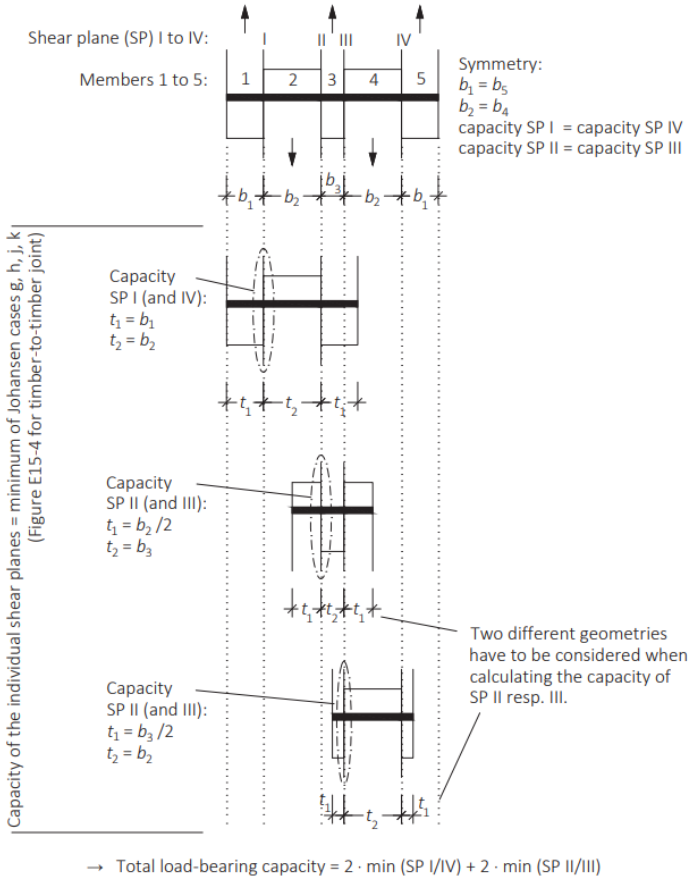

(Blaß & Sandhaas, 2017)

Mode	Strength	Failure mode
I_s	$R_{1k} = f_{h,1,k} t_1 d$	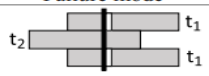
I_m	$R_{2k} = 0.5 f_{h,2,k} t_2 d$	
III_s	$R_{3k} = 1.05 \frac{f_{h,1,k} t_2 d}{2+\beta} \left[\sqrt{2\beta(1+\beta) + \frac{4\beta(2+\beta) M_{y,k}}{f_{h,1,k} d t_1^2}} - \beta \right]$	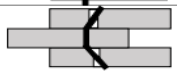
IV	$R_{4k} = 1.15 \sqrt{\frac{2\beta}{1+\beta}} \sqrt{2 M_{y,k} f_{h,1,k} d}$	

($f_{hk,1,k}$, $f_{hk,2}$ = embedding strength of timber; t_1, t_2= boards' thickness; d= fastener's diameter, $M_{y,k}$= characteristic yielding moment of the fastener, $\beta = f_{h,k1}/f_{h,k2}$)

Fig. 4. Strength formulas provided by EYM for double shear plane joints (CEN 2014).

(Sandoli et. al, 2023)

Mode V, in accordance with the model presented in (Miller & Schmidt,2004):

$$f_{vy} = 4810 G_{peg}^{0,926} G_{base}^{0,778} \qquad [psi]$$

$$-yielding\ shear\ capasity\ of\ the\ dowel$$

$Where\ G\ is\ referred\ to\ as\ specific\ gravity$

All calculations are done in accordance with theory presented in (Sandoli et. al, 2023) and (Miller & Shmidt, 2004).

Properties

Total load bearing capacity for 4 shear planes:

$$F_{v,Rk} = 2 * F_{v,R,1,4} + 2 * min \begin{cases} F_{v,R,2,3,1} \\ F_{v,R,2,3,2} \end{cases}$$

Where:

$$F_{v,R,1,4} = Load\ bearing\ capasity\ for\ SP1\ and\ SP4$$

$$F_{v,R,2,3,1} = Load\ bearing\ capasity\ for\ SP2\ and\ SP3\ for\ geometry\ 1$$

$$F_{v,R,2,3,2} = Load\ bearing\ capasity\ for\ SP2\ and\ SP3\ for\ geometry\ 2$$

Glulam Properties:	
Density:	$\rho_{gl} = 390\ kg/m^3$
Mean density:	$\rho_{gl,mean} = \cdots\ kg/m^3$
Thickness:	t = 90 mm
Embedment strength with screws (parallel to grain):	$f_{h,o,k} = 0{,}082 * (1 - 0{,}01d) * \rho_b$
Embedment strength with wood dowels:	$f_{h,0,k} = \rho_b \rho_p * 10^{-4} * 1{,}222(1 - 0{,}011d)$
	$\rho_b = base\ member\ density$
	$\rho_p = peg\ density$
	$d = diameter\ of\ peg/screw$

Plywood properties:	
Density:	$\rho_{pl} = 680\ kg/m^3$
Mean density:	$\rho_{pl,mean} = \cdots\ kg/m^3$
Thickness:	t = 21 mm
Embedment strength with screws:	$f_{h,k} = 0{,}11 * (1 - 0{,}01d) * \rho_b$
Embedment strength with wood dowels:	$f_{h,0,k} = \rho_b \rho_p * 10^{-4} * 1{,}222(1 - 0{,}011d)$
	$\rho_b = base\ member\ density$
	$\rho_p = peg\ density$
	$d = diameter\ of\ peg/screw$

Screw properties:

GEOMETRY AND MECHANICAL CHARACTERISTICS

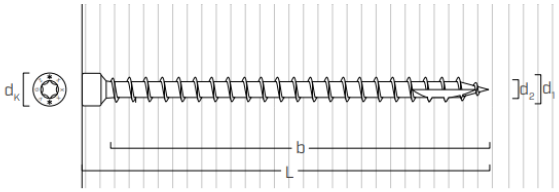

Nominal diameter	d_1	[mm]	5,3	5,6	7	9	11
Head diameter	d_K	[mm]	8,00	8,00	9,50	11,50	13,50
Tip diameter	d_2	[mm]	3,60	3,80	4,60	5,90	6,60
Pre-drilling hole diameter(1)	d_V	[mm]	3,5	3,5	4,0	5,0	6,0
Characteristic yield moment	$M_{y,k}$	[Nm]	9,2	10,6	14,2	27,2	45,9
Characteristic withdrawal-resistance parameter(2)	$f_{ax,k}$	[N/mm²]	11,7	11,7	11,7	11,7	11,7
Associated density	ρ_a	[kg/m³]	350	350	350	350	350
Characteristic withdrawal-resistance parameter(3)	$f_{ax,k}$	[N/mm²]	15,0	15,0	15,0	15,0	15,0
Associated density	ρ_a	[kg/m³]	500	500	500	500	500
Characteristic tensile strength	$f_{tens,k}$	[kN]	11,0	12,3	15,4	25,4	38,0
Characteristic yield strength	$f_{y,k}$	[N/mm²]	1000	1000	1000	1000	1000

(1) Pre-drilling valid for softwood.
(2) Valid for softwood - maximum density 440 kg/m³.
(3) Valid for softwood LVL - maximum density 550 kg/m³.
For applications with different materials or with high density please see ETA-11/0030.

Diameter: $d = 9\ mm$

Yield moment: $M_{y,Rk} = 27{,}2\ Nm = 27200\ Nmm$

Withdrawal capacity: $f_{ax,k} = 11{,}7\ N/mm^2$

Birch Dowel Properties:

Diameter: $d = 20\ mm$

Density: $\rho_p = 650\ \frac{kg}{m^3}$ (see table below)

Mean density: $\rho_{p,mean} = \cdots \frac{kg}{m^3}$

Bending strength: $f_{m,k} = 147\ MPa$ (see table below)

Compressive strength: $f_{c,0,m} = 50\ MPa$ (see link below)

Table 2. Properties of Beech and Birch Woods.

	Wood Species [1]					
	Beech			Birch		
	Min.	Mean	Max.	Min.	Mean	Max.
Density (kg/m^3)	540	720	910	510	650	830
Static modulus of elasticity (MPa)	10,000	16,000	18,000	14,500		16,500
Bending strength (MPa)	74	123	210	76	147	155
Impact bending strength (J/cm^2)	3.0	10.0	19.0	4.5	10.0	13.0
Hardness LR/LT (MPa)		34		22		27

[1] Moisture content 12–15% [38]. LR = radial plane, LT = tangential plane.

(Boruvka et al., 2018)

Laminated Densified Wood Dowels properties:

Diameter: $d = 20\ mm$

Density: $\rho = 1350\,\frac{kg}{m^3}$

Bending strength: $f_{m,k} = 200\ MPa$

Compressive strength parallel to grain: $f_{c,0,m} = 90\ MPa$

Calculation of the estimated force for the birch dowel tests.

BD-test:

Embedment strength with glulam as base material:

$$f_{h,0,k,gl} = \rho_{gl}\rho_p * 10^{-4} * 1{,}222(1 - 0{,}011d)$$

$$= 24{,}16\ N/mm^2$$

Embedment strength with plywood as base material:

$$f_{h,0,k,pl} = \rho_{pl}\rho_p * 10^{-4} * 1{,}222(1 - 0{,}011d)$$

$$= 42{,}13\ N/mm^2$$

Yielding moment:

$$M_{y,k} = 0{,}3 * f_{c,0,m} * d^{2,6}$$

$$= 36205{,}06\ Nmm$$

SP1 and SP4:

$t_1 = 21\ mm \quad t_2 = 90\ mm \quad \beta = \frac{f_{h,0,k,pl}}{f_{h,0,k,gl}} = 1{,}744$

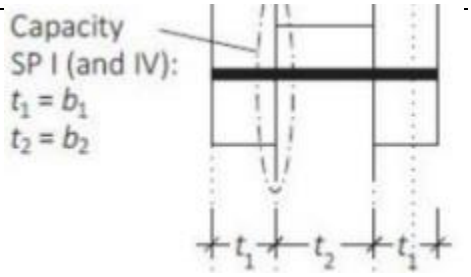

$R_{1,k} = f_{h,0,k,pl} * t_1 * d = 17{,}695\ kN$

$R_{2k} = 0{,}5 * f_{h,0,k,gl} * t_2 * d = 21{,}744\ kN$

$R_{3k} = 1{,}05 * \frac{f_{h,0,k,pl} * t_2 * d}{2+\beta}\left[\sqrt{2\beta(1+\beta) + \frac{4\beta(2+\beta)M_{y,k}}{f_{h,0,k,pl} * d * t_1^2}} - \beta\right] = 36{,}937\ kN$

$R_{4k} = 1{,}15 * \sqrt{\frac{2\beta}{1+\beta}} * \sqrt{2 * M_{y,k} * f_{h,0,k,pl} * d} = 10{,}128\ kN$

$$f_{v,R,1,4} = min\begin{cases} R_{1k} \\ R_{2k} \\ R_{3k} \\ R_{4k} \end{cases} = R_{4k} = 10{,}128\ kN$$

SP2 and SP3, geometry 1:

$f_{h,1} = f_{h,0,k,gl} = 24{,}16\ MPa, f_{h,2} = f_{h,0,k,pl} = 42{,}13\ MPa,$ $t_1 = \frac{t_{gl}}{2} = 45\ mm,$

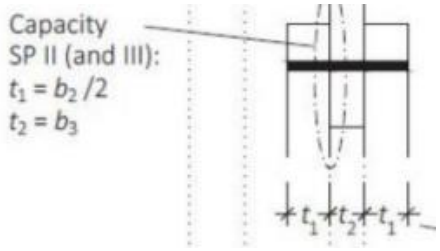

$t_2 = 2 * t_{pl} = 42mm,$ $\beta = \frac{f_{h,1}}{f_{h,2}} = 0{,}573$

$R_{1k} = f_{h,1} * t_1 * d = 21{,}744\ kN$

$R_{2k} = 0{,}5 * f_{h,2} * t_2 * d = 17{,}695\ kN$

$R_{3k} = 1{,}05 * \frac{f_{h,1} * t_2 * d}{2+\beta}\left[\sqrt{2\beta(1+\beta) + \frac{4\beta(2+\beta)M_{y,k}}{f_{h,1} * d * t_1^2}} - \beta\right] = 7{,}028\ kN$

$R_{4k} = 1{,}15 * \sqrt{\frac{2\beta}{1+\beta}} * \sqrt{2 * M_{y,k} * f_{h,1} * d} = 5{,}806\ kN$

$$f_{v,R,2,3,1} = min\begin{cases} R_{1k} \\ R_{2k} \\ R_{3k} \\ R_{4k} \end{cases} = R_{4k} = 5{,}806\ kN$$

SP2 and SP3, geometry 2:

$f_{h,1} = f_{h,0,k,pl} = 42{,}13\ MPa, f_{h,2} = f_{h,0,k,gl} = 24{,}16\ MPa, t_1 = t_{pl} = 21\ mm,$

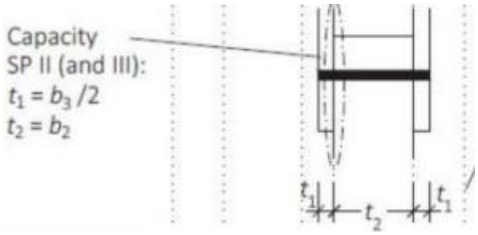

$t_2 = t_{gl} = 90mm,$ $\beta = \frac{f_{h,1}}{f_{h,2}} = 1{,}744$

$R_{1k} = f_{h,1} * t_1 * d = 17{,}695\ kN$

$R_{2k} = 0{,}5 * f_{h,2} * t_2 * d = 21{,}744\ kN$

$R_{3k} = 1{,}05 * \frac{f_{h,1} * t_2 * d}{2+\beta}\left[\sqrt{2\beta(1+\beta) + \frac{4\beta(2+\beta)M_{y,k}}{f_{h,1} * d * t_1^2}} - \beta\right] = 36{,}937\ kN$

$$R_{4k} = 1{,}15 * \sqrt{\frac{2\beta}{1+\beta}} * \sqrt{2 * M_{y,k} * f_{h,1} * d} = 10{,}128\ kN$$

$$f_{v,R,2,3,2} = min \begin{cases} R_{1k} \\ R_{2k} \\ R_{3k} \\ R_{4k} \end{cases} = R_{4k} = 10{,}128\ kN$$

TOTAL LOAD BEARING CAPACITY PER DOWEL:

$F_{v,Rk} = 2 * F_{v,R,1,4} + 2 * F_{v,R,2,3,1} = 31{,}868\ kN$ (Per dowel)

$$\boldsymbol{F_{est,BD} = 2\ dowels * F_{v,Rk} = 63{,}736\ kN}$$

Where:

$$F_{est,BD} \sim estimated\ capacity\ for\ the\ birch\ dowel\ tension\ test$$

Shear failure in the dowel:

$$F_{yv} = 4810 * \left(\frac{650}{1000}\right)^{0{,}926} * \left(\frac{680}{1000}\right)^{0{,}778} = 2391\ psi$$

1 psi = 0,00689 MPa → f_{yv} = 16,47399 MPa

The corresponding shear capacity of the dowel can be calculated by multiplying the shear strength with the cross-sectional area of the dowel.

$F_v = f_{yv} * \frac{d^2 * \pi}{4} = 5{,}175\ kN$ per dowel per shear plane

The total shear capacity of the connection would be:

$$F_v * 4\ shear\ planes = 20{,}702\ kN\ per\ dowel$$

$$\rightarrow F_{est,v} = 20{,}702 \frac{kN}{dowel} * 2\ dowels = 41{,}404\ kN$$

Calculation of the estimated force for the screws

Capacities is gathered from Rothoblaas' own data sheet for the VGZ screws. For the capacities with screws as fasteners the rope effect needs to be accounted for.

Embedment strength Glulam:

$$f_{h,o,k,gl} = 0{,}082 * (1 - 0{,}01d) * \rho_{gl} = 29{,}102\ N/mm^2$$

Embedment strength Plywood:

$$f_{h,0,k,pl} = 0{,}11 * (1 - 0{,}01d) * \rho_{pl} = 68{,}068\ N/mm^2$$

Rope effect:

$$F_{ax,Rk} = \frac{n_{ef} * f_{ax,k} * d * l_{ef} * k_d}{1{,}2 * \cos^2\alpha + \sin^2\alpha}$$

Where:

$n_{ef} = 1 = number\ of\ screws$

$f_{ax,k} = 11{,}7\frac{N}{mm^2} = the\ caractaristic\ withdrawl\ capacity$

$d = 9\ mm = diameter$

$l_{ef} = threaded\ depth\ of\ the\ threaded\ part\ of\ the\ screw$

$k_d = min\begin{cases} d/8 \\ 1{,}0 \end{cases} = 1{,}0\ for\ a\ 9mm\ screw$

SP1 and SP4:

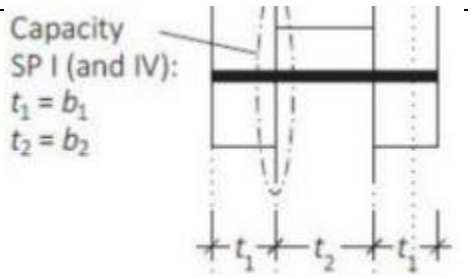

$f_{h,1} = f_{h,0,k,pl} = 68{,}068\ N/mm^2$

$f_{h,2} = f_{h,0,k,gl} = 29{,}102\ N/mm^2$

$t_1 = 21\ mm \quad t_2 = 90\ mm \quad \beta = \frac{f_{h,1}}{f_{h,2}} = 2{,}339$

Rope effect:

$l_{ef} = 2 * t_1 + t_2 = 132\ mm$

$\alpha = 0°$

$F_{ax,Rk} = \frac{n_{ef} * f_{ax,k} * d * l_{ef} * k_d}{1{,}2 * \cos^2\alpha + \sin^2\alpha} = \frac{1 * 11{,}7 * 9 * 132 * 1}{1{,}2 * \cos^2 0 + \sin^2 0} = 11583\ N$

$R_{1k} = f_{h,1} * t_1 * d = 12{,}865\ kN$

$R_{2k} = 0{,}5 * f_{h,2} * t_2 * d = 11{,}786\ kN$

$R_{3k} = 1{,}05 * \frac{f_{h,1} * t_1 * d}{2+\beta} \left[\sqrt{2\beta(1+\beta) + \frac{4\beta(2+\beta) M_{y,k}}{f_{h,1} * d * t_1^2}} - \beta \right] + \frac{F_{ax,Rk}}{4} = 9{,}434\ kN$

$R_{4k} = 1{,}15 * \sqrt{\frac{2\beta}{1+\beta}} * \sqrt{2 * M_{y,k} * f_{h,1} * d} + \frac{F_{ax,Rk}}{4} = 10{,}754\ kN$

$$f_{v,R,1,4} = min \begin{cases} R_{1k} \\ R_{2k} \\ R_{3k} \\ R_{4k} \end{cases} = R_{3k} = 9{,}434\ kN$$

SP2 and SP3 Geometry 1

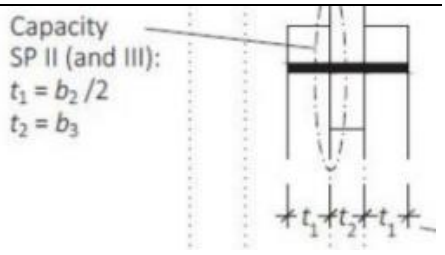

$f_{h,1} = f_{h,0,k,gl} = 29{,}102\ N/mm^2$

$f_{h,2} = f_{h,0,k,pl} = 68{,}068\ N/mm^2$

$t_1 = 45\ mm \quad t_2 = 42\ mm \quad \beta = \frac{f_{h,0,k,gl}}{f_{h,0,k,pl}} = 0{,}428$

Rope effect:

$l_{ef} = 2 * t_1 + t_2 = 132\ mm$

$\alpha = 0°$

$F_{ax,Rk} = \frac{n_{ef} * f_{ax,k} * d * l_{ef} * k_d}{1{,}2 * \cos^2 \alpha + \sin^2 \alpha} = \frac{1 * 11{,}7 * 9 * 132 * 1}{1{,}2 * \cos^2 0 + \sin^2 0} = 11583\ N$

$R_{1k} = f_{h,1} * t_1 * d = 11{,}786\ kN$

$R_{2k} = 0{,}5 * f_{h,2} * t_2 * d = 12{,}865\ kN$

$R_{3k} = 1{,}05 * \frac{f_{h,1} * t_1 * d}{2+\beta} \left[\sqrt{2\beta(1+\beta) + \frac{4\beta(2+\beta) M_{y,k}}{f_{h,1} * d * t_1^2}} - \beta \right] + \frac{F_{ax,Rk}}{4} = 6{,}821\ kN$

$R_{4k} = 1{,}15 * \sqrt{\frac{2\beta}{1+\beta}} * \sqrt{2 * M_{y,k} * f_{h,1} * d} + \frac{F_{ax,Rk}}{4} = 6{,}257\ kN$

$$f_{v,R,2,3,1} = min \begin{cases} R_{1k} \\ R_{2k} \\ R_{3k} \\ R_{4k} \end{cases} = R_{4k} = 6{,}257\ kN$$

SP2 and SP3 Geometry 2

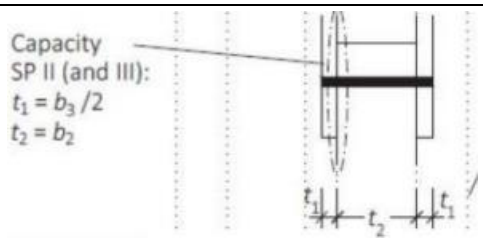

$f_{h,1} = f_{h,0,k,pl} = 68{,}068\ N/mm^2$

$f_{h,2} = f_{h,0,k,gl} = 29{,}102\ N/mm^2$

$t_1 = 21\ mm \quad t_2 = 90\ mm \quad \beta = \frac{f_{h,1}}{f_{h,2}} = 2{,}339$

Rope effect:

$l_{ef} = 2 * t_1 + t_2 = 132\ mm$

$\alpha = 0°$

$F_{ax,Rk} = \frac{n_{ef} * f_{ax,k} * d * l_{ef} * k_d}{1{,}2 * \cos^2 \alpha + \sin^2 \alpha} = \frac{1 * 11{,}7 * 9 * 132 * 1}{1{,}2 * \cos^2 0 + \sin^2 0} = 11583\ N$

$R_{1k} = f_{h,1} * t_1 * d = 12{,}865\ kN$

$$R_{2k} = 0{,}5 * f_{h,2} * t_2 * d = 11{,}786\ kN$$

$$R_{3k} = 1{,}05 * \frac{f_{h,1} * t_1 * d}{2+\beta}\left[\sqrt{2\beta(1+\beta) + \frac{4\beta(2+\beta)M_{y,k}}{f_{h,1} * d * t_1^2}} - \beta\right] + \frac{F_{ax,Rk}}{4} = 9{,}434\ kN$$

$$R_{4k} = 1{,}15 * \sqrt{\frac{2\beta}{1+\beta}} * \sqrt{2 * M_{y,k} * f_{h,1} * d} + \frac{F_{ax,Rk}}{4} = 10{,}754\ kN$$

$$f_{v,R,2,3,2} = min\begin{cases} R_{1k} \\ R_{2k} \\ R_{3k} \\ R_{4k} \end{cases} = R_{3k} = 9{,}434\ kN$$

TOTAL LOAD BEARING CAPACITY PER SCREW:

$F_{v,Rk} = 2 * F_{v,R,1,4} + 2 * F_{v,R,2,3,1} = 31{,}382\ kN$ (Per screw)

$$\boldsymbol{F_{est,S} = 2\ screws * F_{v,Rk} = 62{,}764\ kN}$$

Where:

$F_{est,S} \sim estimated\ capacity\ for\ the\ tests\ with\ steel\ screws$

Calculation of the estimated force for the LDW tests.

LDW-test:

Embedment strength with glulam as base material:

$$f_{h,0,k,gl} = \rho_{gl}\rho_p * 10^{-4} * 1{,}222(1 - 0{,}011d)$$

$$= 50{,}18\ N/mm^2$$

Embedment strength with plywood as base material:

$$f_{h,0,k,pl} = \rho_{pl}\rho_p * 10^{-4} * 1{,}222(1 - 0{,}011d)$$

$$= 87{,}50\ N/mm^2$$

Yielding moment:

$$M_{y,k} = 0{,}3 * f_{c,0,m} * d^{2,6}$$

$$= 65169{,}10\ Nmm$$

SP1 and SP4:

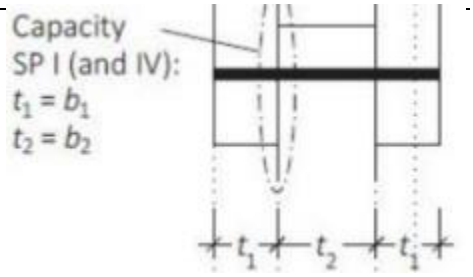

$t_1 = 21\ mm \quad t_2 = 90\ mm \quad \beta = \frac{f_{h,0,k,pl}}{f_{h,0,k,gl}} = 1{,}744$

$$f_{h,0,k,pl} = f_{h,1} = 87{,}50\ N/mm^2$$

$$f_{h,0,k,gl} = f_{h,2} = 50{,}18\ N/mm^2$$

$R_{1,k} = f_{h,1} * t_1 * d = 36{,}750\ kN$

$R_{2k} = 0{,}5 * f_{h,2} * t_2 * d = 45{,}162\ kN$

$R_{3k} = 1{,}05 * \frac{f_{h,1} * t_2 * d}{2+\beta}\left[\sqrt{2\beta(1+\beta) + \frac{4\beta(2+\beta)M_{y,k}}{f_{h,1} * d * t_1^2}} - \beta\right] = 74{,}547\ kN$

$R_{4k} = 1{,}15 * \sqrt{\frac{2\beta}{1+\beta}} * \sqrt{2 * M_{y,k} * f_{h,1} * d} = 19{,}581\ kN$

$$f_{v,R,1,4} = min\begin{cases} R_{1k} \\ R_{2k} \\ R_{3k} \\ R_{4k} \end{cases} = R_{4k} = 19{,}581\ kN$$

SP2 and SP3, geometry 1:

$f_{h,1} = f_{h,0,k,gl} = 50{,}18\ MPa, f_{h,2} = f_{h,0,k,pl} = 87{,}50\ MPa, t_1 = \frac{t_{gl}}{2} =$ $45\ mm$,

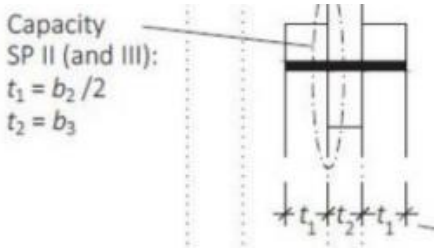

$t_2 = 2 * t_{pl} = 42mm, \qquad \beta = \frac{f_{h,1}}{f_{h,2}} = 0{,}573$

$R_{1k} = f_{h,1} * t_1 * d = 45{,}162\ kN$

$R_{2k} = 0{,}5 * f_{h,2} * t_2 * d = 36{,}750\ kN$

$R_{3k} = 1{,}05 * \frac{f_{h,1} * t_2 * d}{2+\beta}\left[\sqrt{2\beta(1+\beta) + \frac{4\beta(2+\beta)M_{y,k}}{f_{h,1} * d * t_1^2}} - \beta\right] = 14{,}420\ kN$

$R_{4k} = 1{,}15 * \sqrt{\frac{2\beta}{1+\beta}} * \sqrt{2 * M_{y,k} * f_{h,1} * d} = 11{,}226\ kN$

$$f_{v,R,2,3,1} = min\begin{cases} R_{1k} \\ R_{2k} \\ R_{3k} \\ R_{4k} \end{cases} = R_{4k} = 11{,}226\ kN$$

SP2 and SP3, geometry 2:

$f_{h,1} = f_{h,0,k,pl} = 87{,}50\ MPa, f_{h,2} = f_{h,0,k,gl} = 50{,}18\ MPa, t_1 = t_{pl} =$ $21\ mm$,

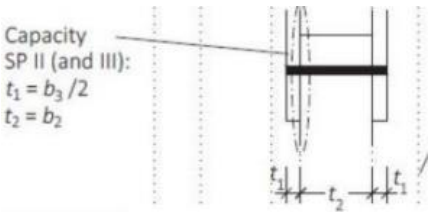

$t_2 = t_{gl} = 90mm, \quad \beta = \frac{f_{h,1}}{f_{h,2}} = 1{,}744$

$R_{1k} = f_{h,1} * t_1 * d = 36{,}750\ kN$

$R_{2k} = 0{,}5 * f_{h,2} * t_2 * d = 45{,}162\ kN$

$R_{3k} = 1{,}05 * \frac{f_{h,1} * t_2 * d}{2+\beta}\left[\sqrt{2\beta(1+\beta) + \frac{4\beta(2+\beta)M_{y,k}}{f_{h,1} * d * t_1^2}} - \beta\right] = 74{,}546\ kN$ $R_{4k} = 1{,}15 * \sqrt{\frac{2\beta}{1+\beta}} * \sqrt{2 * M_{y,k} * f_{h,1} * d} = 19{,}582\ kN$

$$f_{v,R,2,3,2} = min\begin{cases} R_{1k} \\ R_{2k} \\ R_{3k} \\ R_{4k} \end{cases} = R_{4k} = 19{,}582\ kN$$

TOTAL LOAD BEARING CAPACITY PER DOWEL:

$F_{v,Rk} = 2 * F_{v,R,1,4} + 2 * F_{v,R,2,3,1} = 61{,}614\ kN$ (Per dowel)

$\boldsymbol{F_{est,LDW} = 2\ dowels * F_{v,Rk} = 123{,}228\ kN}$

Where:

$F_{est,LDW} \sim estimated\ capacity\ for\ the\ LDW\ tension\ test$

Shear failure in the dowel:

$$F_{yv} = 4810 * \left(\frac{1350}{1000}\right)^{0{,}926} * \left(\frac{680}{1000}\right)^{0{,}778} = 4704{,}6\ psi$$

1 psi = 0,00689 MPa → f_{yv} = 32,4149 MPa

The corresponding shear capacity of the dowel can be calculated by multiplying the shear strength with the cross-sectional area of the dowel.

$F_v = f_{yv} * \frac{d^2 * \pi}{4} = 10{,}183\ kN$ per dowel per shear plane

The total shear capacity of the connection would be:

$$F_v * 4\ shear\ planes = 40{,}734\ kN\ per\ dowel$$

$$\rightarrow F_{est,v} = 20{,}702\frac{kN}{dowel} * 2\ dowels = 81{,}468\ kN$$

Appendix B – Excel Spreadsheets – Moisture Content and Density

Densitet og fuktinnhold av dybler

Specimen	Treslag	ID	vekt	volum	torrvekt	torrvolum	Fuktighet	Densitet
Prototyp	Bøk	1	3.022	4.41			#DIV/0!	685.3
Prototyp	Bøk	2	3.558	5.52			#DIV/0!	644.6
Prototyp	Bøk	3	2.828	4.3			#DIV/0!	657.7
Prototyp	Bøk	4	3.695	5.4			#DIV/0!	684.3
BD-(02)	Bjørk	5	9.324	15.04			#DIV/0!	619.9
BD-(02)	Bjørk	6	13.37	19.55			#DIV/0!	683.9
BD-(02)	Bjørk	7	10.714	15.4			#DIV/0!	695.7
BD-(02)	Bjørk	8	10.625	15.89			#DIV/0!	668.7
BD-(05)	Bjørk	9	9.337	14.79			#DIV/0!	631.3
BD-(05)	Bjørk	10	9.846	15.99			#DIV/0!	615.8
BD-(05)	Bjørk	11	10.619	15.76			#DIV/0!	673.8
BD-(05)	Bjørk	12	11.646	16.4			#DIV/0!	710.1
BD-(04)	Bjørk	13	9.599	15.59			#DIV/0!	615.7
BD-(04)	Bjørk	14	9.396	13.75			#DIV/0!	683.3
BD-(04)	Bjørk	15	10.07	15.84			#DIV/0!	635.7
BD-(04)	Bjørk	16	9.741	14.05			#DIV/0!	693.3
BD-(01)	Bjørk	17	7.809	12.51			#DIV/0!	624.2
BD-(01)	Bjørk	18	7.643	11.12			#DIV/0!	687.3
BD-(01)	Bjørk	19	6.779	9.99			#DIV/0!	678.6
BD-(01)	Bjørk	20	7.711	12.09			#DIV/0!	637.8
BD-(03)	Bjørk	21	10.265	16.29			#DIV/0!	630.1
BD-(03)	Bjørk	22	10.647	14.69			#DIV/0!	724.8
BD-(03)	Bjørk	23	8.778	13.76			#DIV/0!	637.9
BD-(03)	Bjørk	24	9.066	14			#DIV/0!	647.6
Mean values								**659.8**
SD								**31.8**
BD-(03)	Bjørk	?	61		55.4		10.1	
BD-(03)	Bjørk	?	68.83		62.72		9.7	
BD-(03)	Bjørk	?	65.19		59.48		9.6	
BD-(03)	Bjørk	?	61.25		55.67		10.0	
Mean values							**9.9**	
SD							**0.237855**	

Specimen	Treslag	ID	Vekt	torrvekt	Fuktighet	l [mm]	d [mm]	V [m^3]	Densitet [kg/m^3]
LDW-(1)	LDW	5	13.91	13.38	4.0	36.93	19.23	1.07E-05	1296.88
LDW-(1)	LDW	6	14.93	14.5	3.0	38.16	19.24	1.11E-05	1345.71
LDW-(1)	LDW	7	14.61	14.23	2.7	36.91	19.26	1.08E-05	1358.64
LDW-(1)	LDW	8	14.08	13.57	3.8	36.95	19.26	1.08E-05	1307.93
LDW-(2)	LDW	17	14.59	14.25	2.4	36.8	19.25	1.07E-05	1362.25
LDW-(2)	LDW	18	14.55	14.19	2.5	36.61	19.26	1.07E-05	1364.15
LDW-(2)	LDW	19	14.99	14.6	2.7	37.91	19.23	1.1E-05	1361.44
LDW-(2)	LDW	20	14.33	13.91	3.0	36.54	19.25	1.06E-05	1347.49
LDW-(3)	LDW	1	12.71	12.27	3.6	33.21	19.23	9.65E-06	1317.74
LDW-(3)	LDW	2	14.82	14.4	2.9	37.48	19.25	1.09E-05	1358.62
LDW-(3)	LDW	3	14.61	14.24	2.6	36.61	19.26	1.07E-05	1369.77
LDW-(3)	LDW	4	14.65	14.27	2.7	36.81	19.24	1.07E-05	1368.90
LDW-(4)	LDW	9	14.72	14.34	2.6	36.77	19.27	1.07E-05	1372.65
LDW-(4)	LDW	10	14.29	13.84	3.3	36.71	19.23	1.07E-05	1340.29
LDW-(4)	LDW	11	14.59	14.15	3.1	37.31	19.23	1.08E-05	1346.42
LDW-(4)	LDW	12	14.68	14.2	3.4	37.73	19.27	1.1E-05	1334.09
LDW-(5)	LDW	13	14.26	13.79	3.4	37.02	19.24	1.08E-05	1324.90
LDW-(5)	LDW	14	14.4	14.01	2.8	36.92	19.24	1.07E-05	1341.53
LDW-(5)	LDW	15	13.81	13.3	3.8	36.49	19.24	1.06E-05	1301.73
LDW-(5)	LDW	16	14.44	14.04	2.8	36.52	19.25	1.06E-05	1358.58
Mean values					**3.0**				**1343.99**
SD					**0.46786**				**23.27**

Appendix C – Python Scripts

```python
# -*- coding: utf-8 -*-
"""
Created on Mon Jul  3 15:12:07 2023

@author: 47986
"""

import numpy as np
import matplotlib.pyplot as plt
import os


#_____________________________________BD-Tests_____________________________________

# Directory path containing the data files
directory = 'C:/Users/47986/OneDrive/Documents/MASTEROPPGAVE/BD-test/Updated text documents BD'

# List to store the data from all files
all_force = []
all_displacement_1 = []
all_displacement_2 = []
all_displacement_3 = []
all_displacement_4 = []

# Get the list of files sorted by identification number
files = sorted([filename for filename in os.listdir(directory) if filename.endswith('.txt')],
               key=lambda x: int(x.split('_BD_')[1].split('(')[-1].replace(').txt', '')))

# Iterate over sorted files
for filename in files:
    file_path = os.path.join(directory, filename)

    # Load data, skip the header row, replace comma with dot, handle empty strings
    data = np.loadtxt(file_path, delimiter='\t', skiprows=1,
                      converters={i: lambda x: float(x.decode().replace(',', '.')) if x else 0 for i in range(9)},
                      usecols=(1, 3, 4, 5, 6))

    # Extract columns
    force = data[:, 0]
    displacement_1 = np.abs(data[:, 1])  # Change negative values to positive
    displacement_2 = np.abs(data[:, 2])  # Change negative values to positive
    displacement_3 = np.abs(data[:, 3])  # Change negative values to positive
    displacement_4 = np.abs(data[:, 4])  # Change negative values to positive

    # Append data to the lists
    all_force.append(force)
    all_displacement_1.append(displacement_1)
    all_displacement_2.append(displacement_2)
    all_displacement_3.append(displacement_3)
    all_displacement_4.append(displacement_4)
```

```python
# Create the first graph (displacement 1 vs. force)
plt.figure()
for i in range(len(all_force)):
    specimen_number = int(files[i].split('(')[-1].replace(').txt', ''))
    plt.plot(all_displacement_1[i], all_force[i], label=f'BD-({specimen_number})')
    max_force_index = np.argmax(all_force[i])
    plt.scatter(all_displacement_1[i][max_force_index], all_force[i][max_force_index], color='red')
plt.xlabel('Displacement 1 (mm)')
plt.ylabel('Force (kN)')
plt.title('BD-tests, Displacement 1 vs. Force')
plt.xlim(0, 50)
plt.ylim(0, 100)
plt.legend()
plt.axvline(x=15, color='red', linestyle='--')
plt.grid(True)
```

```
67
68  # Move the spines to the bottom and left edges
69  ax = plt.gca()
70  ax.spines['bottom'].set_position('zero')
71  ax.spines['left'].set_position('zero')
72
73  # Hide the top and right spines
74  ax.spines['top'].set_visible(False)
75  ax.spines['right'].set_visible(False)
76
77  # Create the second graph (displacement 2 vs. force)
78  plt.figure()
79  for i in range(len(all_force)):
80      specimen_number = int(files[i].split('(')[-1].replace(').txt', ''))
81      plt.plot(all_displacement_2[i], all_force[i], label=f'BD-({specimen_number})')
82      max_force_index = np.argmax(all_force[i])
83      plt.scatter(all_displacement_2[i][max_force_index], all_force[i][max_force_index], color='red')
84  plt.xlabel('Displacement 2 (mm)')
85  plt.ylabel('Force (kN)')
86  plt.title('BD-tests, Displacement 2 vs. Force')
87  plt.xlim(0, 50)
88  plt.ylim(0, 100)
89  plt.legend()
90  plt.axvline(x=15, color='red', linestyle='--')
91  plt.grid(True)
92
93  # Move the spines to the bottom and left edges
94  ax = plt.gca()
95  ax.spines['bottom'].set_position('zero')
96  ax.spines['left'].set_position('zero')
97
98  # Hide the top and right spines
99  ax.spines['top'].set_visible(False)
100 ax.spines['right'].set_visible(False)
101
102 # Create the third graph (displacement 3 vs. force)
103 plt.figure()
104 for i in range(len(all_force)):
105     specimen_number = int(files[i].split('(')[-1].replace(').txt', ''))
106     plt.plot(all_displacement_3[i], all_force[i], label=f'BD-({specimen_number})')
107     max_force_index = np.argmax(all_force[i])
108     plt.scatter(all_displacement_3[i][max_force_index], all_force[i][max_force_index], color='red')
109 plt.xlabel('Displacement 3 (mm)')
110 plt.ylabel('Force (kN)')
111 plt.title('BD-tests, Displacement 3 vs. Force')
112 plt.xlim(0, 50)
113 plt.ylim(0, 100)
114 plt.legend()
115 plt.axvline(x=15, color='red', linestyle='--')
116 plt.grid(True)
117
```

```
117
118 # Move the spines to the bottom and left edges
119 ax = plt.gca()
120 ax.spines['bottom'].set_position('zero')
121 ax.spines['left'].set_position('zero')
122
123 # Hide the top and right spines
124 ax.spines['top'].set_visible(False)
125 ax.spines['right'].set_visible(False)
126
127 # Create the fourth graph (displacement 4 vs. force)
128 plt.figure()
129 for i in range(len(all_force)):
130     specimen_number = int(files[i].split('(')[-1].replace(').txt', ''))
131     plt.plot(all_displacement_4[i], all_force[i], label=f'BD-({specimen_number})')
132     max_force_index = np.argmax(all_force[i])
133     plt.scatter(all_displacement_4[i][max_force_index], all_force[i][max_force_index], color='red')
134 plt.xlabel('Displacement 4 (mm)')
135 plt.ylabel('Force (kN)')
136 plt.title('BD-tests, Displacement 4 vs. Force')
137 plt.xlim(0, 50)
```

```
plt.ylim(0, 100)
plt.legend()
plt.axvline(x=15, color='red', linestyle='--')
plt.grid(True)

# Move the spines to the bottom and left edges
ax = plt.gca()
ax.spines['bottom'].set_position('zero')
ax.spines['left'].set_position('zero')

# Hide the top and right spines
ax.spines['top'].set_visible(False)
ax.spines['right'].set_visible(False)

# Show all the graphs
plt.show()

#_____________________________________LDW-Tests_____________________________________

# Directory path containing the data files
directory = 'C:/Users/47986/OneDrive/Documents/MASTEROPPGAVE/LDW-test/Text files with results from LDW-tests'

# List to store the data from all files
all_force = []
all_displacement_1 = []
all_displacement_2 = []
all_displacement_3 = []
all_displacement_4 = []

# Get the list of files sorted by identification number
files = sorted([filename for filename in os.listdir(directory) if filename.endswith('.txt')],
               key=lambda x: int(x.split('_LDW_')[1].split('(')[-1].replace(').txt', '')))

# Iterate over sorted files
for filename in files:
    file_path = os.path.join(directory, filename)

    # Load data, skip the header row, replace comma with dot, handle empty strings
    data = np.loadtxt(file_path, delimiter='\t', skiprows=1,
                      converters={i: lambda x: float(x.decode().replace(',', '.')) if x else 0 for i in range(9)},
                      usecols=(1, 3, 4, 5, 6))

    # Extract columns
    force = data[:, 0]
    displacement_1 = np.abs(data[:, 1])  # Change negative values to positive
    displacement_2 = np.abs(data[:, 2])  # Change negative values to positive
    displacement_3 = np.abs(data[:, 3])  # Change negative values to positive
    displacement_4 = np.abs(data[:, 4])  # Change negative values to positive

```

```
    # Append data to the lists
    all_force.append(force)
    all_displacement_1.append(displacement_1)
    all_displacement_2.append(displacement_2)
    all_displacement_3.append(displacement_3)
    all_displacement_4.append(displacement_4)

# Create the first graph (displacement 1 vs. force)
plt.figure()
for i in range(len(all_force)):
    specimen_number = int(files[i].split('(')[-1].replace(').txt', ''))
    plt.plot(all_displacement_1[i], all_force[i], label=f'LDW-({specimen_number})')
    max_force_index = np.argmax(all_force[i])
    plt.scatter(all_displacement_1[i][max_force_index], all_force[i][max_force_index], color='red')
plt.xlabel('Displacement 1 (mm)')
plt.ylabel('Force (kN)')
plt.title('LDW-tests, Displacement 1 vs. Force')
plt.xlim(0, 50)
plt.ylim(0, 100)
plt.legend()
plt.axvline(x=15, color='red', linestyle='--')
plt.grid(True)
```

```
# Move the spines to the bottom and left edges
ax = plt.gca()
ax.spines['bottom'].set_position('zero')
ax.spines['left'].set_position('zero')

# Hide the top and right spines
ax.spines['top'].set_visible(False)
ax.spines['right'].set_visible(False)

# Create the second graph (displacement 2 vs. force)
plt.figure()
for i in range(len(all_force)):
    specimen_number = int(files[i].split('(')[-1].replace(').txt', ''))
    plt.plot(all_displacement_2[i], all_force[i], label=f'LDW-({specimen_number})')
    max_force_index = np.argmax(all_force[i])
    plt.scatter(all_displacement_2[i][max_force_index], all_force[i][max_force_index], color='red')
plt.xlabel('Displacement 2 (mm)')
plt.ylabel('Force (kN)')
plt.title('LDW-tests, Displacement 2 vs. Force')
plt.xlim(0, 50)
plt.ylim(0, 100)
plt.legend()
plt.axvline(x=15, color='red', linestyle='--')
plt.grid(True)

# Move the spines to the bottom and left edges
ax = plt.gca()
ax.spines['bottom'].set_position('zero')
ax.spines['left'].set_position('zero')

# Hide the top and right spines
ax.spines['top'].set_visible(False)
ax.spines['right'].set_visible(False)

# Create the third graph (displacement 3 vs. force)
plt.figure()
for i in range(len(all_force)):
    specimen_number = int(files[i].split('(')[-1].replace(').txt', ''))
    plt.plot(all_displacement_3[i], all_force[i], label=f'LDW-({specimen_number})')
    max_force_index = np.argmax(all_force[i])
    plt.scatter(all_displacement_3[i][max_force_index], all_force[i][max_force_index], color='red')
plt.xlabel('Displacement 3 (mm)')
plt.ylabel('Force (kN)')
plt.title('LDW-tests, Displacement 3 vs. Force')
plt.xlim(0, 50)
plt.ylim(0, 100)
plt.legend()
plt.axvline(x=15, color='red', linestyle='--')
plt.grid(True)

```

```
# Move the spines to the bottom and left edges
ax = plt.gca()
ax.spines['bottom'].set_position('zero')
ax.spines['left'].set_position('zero')

# Hide the top and right spines
ax.spines['top'].set_visible(False)
ax.spines['right'].set_visible(False)

# Create the fourth graph (displacement 4 vs. force)
plt.figure()
for i in range(len(all_force)):
    specimen_number = int(files[i].split('(')[-1].replace(').txt', ''))
    plt.plot(all_displacement_4[i], all_force[i], label=f'LDW-({specimen_number})')
    max_force_index = np.argmax(all_force[i])
    plt.scatter(all_displacement_4[i][max_force_index], all_force[i][max_force_index], color='red')
plt.xlabel('Displacement 4 (mm)')
plt.ylabel('Force (kN)')
plt.title('LDW-tests, Displacement 4 vs. Force')
plt.xlim(0, 50)
plt.ylim(0, 100)
plt.legend()
plt.axvline(x=15, color='red', linestyle='--')
plt.grid(True)
```

```python
# Move the spines to the bottom and left edges
ax = plt.gca()
ax.spines['bottom'].set_position('zero')
ax.spines['left'].set_position('zero')

# Hide the top and right spines
ax.spines['top'].set_visible(False)
ax.spines['right'].set_visible(False)

# Show all the graphs
plt.show()

#_____________________________________S-Tests_____________________________________

# Directory path containing the data files
directory = 'C:/Users/47986/OneDrive/Documents/MASTEROPPGAVE/S-test/Text files with results from the S-tests'

# List to store the data from all files
all_force = []
all_displacement_1 = []
all_displacement_2 = []
all_displacement_3 = []
all_displacement_4 = []

# Get the list of files sorted by identification number
files = sorted([filename for filename in os.listdir(directory) if filename.endswith('.txt')],
               key=lambda x: int(x.split('_S_')[1].split('(')[-1].replace(').txt', '')))

# Iterate over sorted files
for filename in files:
    file_path = os.path.join(directory, filename)

    # Load data, skip the header row, replace comma with dot, handle empty strings
    data = np.loadtxt(file_path, delimiter='\t', skiprows=1,
                      converters={i: lambda x: float(x.decode().replace(',', '.')) if x else 0 for i in range(9)},
                      usecols=(1, 3, 4, 5, 6))

    # Extract columns
    force = data[:, 0]
    displacement_1 = np.abs(data[:, 1])  # Change negative values to positive
    displacement_2 = np.abs(data[:, 2])  # Change negative values to positive
    displacement_3 = np.abs(data[:, 3])  # Change negative values to positive
    displacement_4 = np.abs(data[:, 4])  # Change negative values to positive

    # Append data to the lists
    all_force.append(force)
    all_displacement_1.append(displacement_1)
    all_displacement_2.append(displacement_2)
    all_displacement_3.append(displacement_3)
    all_displacement_4.append(displacement_4)
```

```python
# Create the first graph (displacement 1 vs. force)
plt.figure()
for i in range(len(all_force)):
    specimen_number = int(files[i].split('(')[-1].replace(').txt', ''))
    plt.plot(all_displacement_1[i], all_force[i], label=f'S-({specimen_number})')
    max_force_index = np.argmax(all_force[i])
    plt.scatter(all_displacement_1[i][max_force_index], all_force[i][max_force_index], color='red')
plt.xlabel('Displacement 1 (mm)')
plt.ylabel('Force (kN)')
plt.title('S-tests, Displacement 1 vs. Force')
plt.xlim(0, 50)
plt.ylim(0, 100)
plt.legend()
plt.axvline(x=15, color='red', linestyle='--')
plt.grid(True)

# Move the spines to the bottom and left edges
ax = plt.gca()
ax.spines['bottom'].set_position('zero')
ax.spines['left'].set_position('zero')

# Hide the top and right spines
ax.spines['top'].set_visible(False)
ax.spines['right'].set_visible(False)

```

```
# Create the second graph (displacement 2 vs. force)
plt.figure()
for i in range(len(all_force)):
    specimen_number = int(files[i].split('(')[-1].replace(').txt', ''))
    plt.plot(all_displacement_2[i], all_force[i], label=f'S-({specimen_number})')
    max_force_index = np.argmax(all_force[i])
    plt.scatter(all_displacement_2[i][max_force_index], all_force[i][max_force_index], color='red')
plt.xlabel('Displacement 2 (mm)')
plt.ylabel('Force (kN)')
plt.title('S-tests, Displacement 2 vs. Force')
plt.xlim(0, 50)
plt.ylim(0, 100)
plt.legend()
plt.axvline(x=15, color='red', linestyle='--')
plt.grid(True)

# Move the spines to the bottom and left edges
ax = plt.gca()
ax.spines['bottom'].set_position('zero')
ax.spines['left'].set_position('zero')

# Hide the top and right spines
ax.spines['top'].set_visible(False)
ax.spines['right'].set_visible(False)

# Create the third graph (displacement 3 vs. force)
plt.figure()
for i in range(len(all_force)):
    specimen_number = int(files[i].split('(')[-1].replace(').txt', ''))
    plt.plot(all_displacement_3[i], all_force[i], label=f'S-({specimen_number})')
    max_force_index = np.argmax(all_force[i])
    plt.scatter(all_displacement_3[i][max_force_index], all_force[i][max_force_index], color='red')
plt.xlabel('Displacement 3 (mm)')
plt.ylabel('Force (kN)')
plt.title('S-tests, Displacement 3 vs. Force')
plt.xlim(0, 50)
plt.ylim(0, 100)
plt.legend()
plt.axvline(x=15, color='red', linestyle='--')
plt.grid(True)

# Move the spines to the bottom and left edges
ax = plt.gca()
ax.spines['bottom'].set_position('zero')
ax.spines['left'].set_position('zero')

# Hide the top and right spines
ax.spines['top'].set_visible(False)
ax.spines['right'].set_visible(False)

```

```
# Create the fourth graph (displacement 4 vs. force)
plt.figure()
for i in range(len(all_force)):
    specimen_number = int(files[i].split('(')[-1].replace(').txt', ''))
    plt.plot(all_displacement_4[i], all_force[i], label=f'S-({specimen_number})')
    max_force_index = np.argmax(all_force[i])
    plt.scatter(all_displacement_4[i][max_force_index], all_force[i][max_force_index], color='red')
plt.xlabel('Displacement 4 (mm)')
plt.ylabel('Force (kN)')
plt.title('S-tests, Displacement 4 vs. Force')
plt.xlim(0, 50)
plt.ylim(0, 100)
plt.legend()
plt.axvline(x=15, color='red', linestyle='--')
plt.grid(True)

# Move the spines to the bottom and left edges
ax = plt.gca()
ax.spines['bottom'].set_position('zero')
ax.spines['left'].set_position('zero')

# Hide the top and right spines
ax.spines['top'].set_visible(False)
ax.spines['right'].set_visible(False)

# Show all the graphs
plt.show()
```

Norges miljø- og biovitenskapelige universitet
Noregs miljø- og biovitskapelege universitet
Norwegian University of Life Sciences

Postboks 5003
NO-1432 Ås
Norway